

## Article

# Late Quaternary Dynamics of Landscape and Climate in the North of the West Siberian Plain Revealed by Paleoecological Studies of Peat and Lake Sediments

Tatina Blyakharchuk <sup>1,2,\*</sup>, Nikita Shefer <sup>1,2</sup>, Olga Ponomareva <sup>3,4</sup> and Hong-Chun Li <sup>5</sup>

<sup>1</sup> Institute of Monitoring of Climatic and Ecological Systems Siberian Branch of the Russian Academy of Sciences, Akademicheskii ave. 10/3, 634055 Tomsk, Russia; vchifz@mail.ru (N.S.)

<sup>2</sup> Department of Geography and Biological Institute, Tomsk State University, Lenina 36, 634050 Tomsk, Russia

<sup>3</sup> Earth Cryosphere Institute Tyumen Scientific Centre Siberian Branch of the Russian Academy of Sciences, Tyumen Scientific Center, 625026 Tyumen, Russia; o-ponomareva@yandex.ru

<sup>4</sup> Department of Engineering Geology, Federal State Budgetary Educational Institution of Higher Education "Sergo Ordzhonikidze Russian State University for Geological Prospecting", 117485 Moscow, Russia

<sup>5</sup> Department of Geosciences, National Taiwan University, Taipei 106, Taiwan; hcli1960@ntu.edu.tw

\* Correspondence: blyakharchuk@mail.ru

**Abstract:** West Siberian mires covering more than 50% of area in the subarctic are still poorly investigated despite their thick peat sediments suitable for paleogeographic research of past long-term landscape and climatic changes. In this research, a combination of paleoecological methods were used, including the analysis of pollen, spores, diatoms, NPPs, and macrofossils, the measurement of peat humification, and quantitative paleoclimate reconstruction. This multi-proxy approach was applied to study a palsa bog (frost peat heave mound) located in the north of western Siberia on the border of the northern taiga and forest-tundra (65°18'56" N, 72°52'27" E). Chronology is based on 21 radiocarbon dates, which were calibrated in CLAM. Studies have shown that sediments of palsa bog Nadym of a 1050 cm thickness were formed both in the Holocene and earlier periods of the Quaternary. Radiocarbon dating worked well for peat sequences (610 cm thick), but failed for underlying lacustrine and mineral sediments (440 cm thick). Numerous remains of salt-water diatoms and exotic Neogene pollen were found in the lacustrine sediments (650–850 cm). The oldest sediments (850–1050 cm) have signs of secondary epicryogenic diagenesis in the form of cryogenic iron-enriched granules. Both lacustrine and bottom sediments contain abundant coniferous pollen. At the same time, spore-pollen complexes dated to the Last Glacial Age were not found in low sediments because of failed dates. To explain this, the authors turn to the hypothesis of glyacioisostatic compensation, according to which the study area was uplifted during the Last Glacial Age and the ancient deposits underwent secondary diagenesis in subaerial conditions. Holocene lacustrine sedimentation began to form about 9800 cal. a BP. These lacustrine sediments turned out to be enriched in redeposited Neogene pollen and diatoms. It was interpreted as an influence of excess humid climate in combination with geological subsidence of landscape in the study area during the Early Holocene. This caused lake formation and introduction of exotic microfossils via surface run-off from higher-relief areas in the catchment. Syngenetic sedimentation in the Nadym section is associated only with peat-mire deposits covering the last 8400 cal. a BP. For this time, the dynamic of vegetation cover and quantitative changes in paleoclimate were reconstructed using spore-pollen, macrofossil, humus, and NPP data as well as the information-statistical method of V.A. Klimanov. The spore-pollen analysis revealed four main phases in the development of vegetation cover: 1. Spruce-birch forests with open meadows and lakes (8400–7600 cal. a BP); 2. Dominance of spruce forests and thawed eutrophic (minerotrophic) mires (7600 to 6500 cal. a BP); 3. Coniferous-birch forests and thawed mesotrophic mires (6500 to 4500 cal. a BP); 4. Birch-pine forests and oligotrophic (ombrotrophic) bogs with permafrost mounds—palsa bogs (approx. the last 4500 years). Quantitative reconstructions of paleoclimate based on pollen data show that in most cases the periods of a sharp decrease in mean January and mean July temperatures coincided with episodes of low solar activity. The assumption was made about the determining influence of solar activity on the formation of permafrost in the soils and mires of the study area. Sun



**Citation:** Blyakharchuk, T.; Shefer, N.; Ponomareva, O.; Li, H.-C. Late Quaternary Dynamics of Landscape and Climate in the North of the West Siberian Plain Revealed by Paleoecological Studies of Peat and Lake Sediments. *Quaternary* **2024**, *7*, 1. <https://doi.org/10.3390/quat7010001>

Academic Editors: Dávid Molnár and Henry Lamb

Received: 5 June 2023

Revised: 30 August 2023

Accepted: 28 November 2023

Published: 22 December 2023



**Copyright:** © 2023 by the authors. Licensee MDPI, Basel, Switzerland. This article is an open access article distributed under the terms and conditions of the Creative Commons Attribution (CC BY) license (<https://creativecommons.org/licenses/by/4.0/>).

minima caused permafrost formation in the mire periodically since 8400 cal. a BP in study peatland, but complete freezing of the peat mire and formation of the palsa bog occurred at c. 2800 cal. a BP.

**Keywords:** spore–pollen analysis; peat; mire; vegetation cover; change in climate; frost peat heave mound; western Siberia; permafrost

## 1. Introduction

Arctic and subarctic nature is very vulnerable and unstable toward climatic changes and technogenic influence, which can cause degradation of northern natural systems and unpredictable consequences at the global level [1,2]. Meanwhile, during the past 25 years, an actual problem became the problem of global warming of climate, noted by the Intergovernmental Group of Experts of Organization of United Nations for problems of climatic changes, as one of the important problems of modern human society [3]. Based on the opinion of experts, stronger warming is expected at high altitudes. One of the reasons for this warming can be an anthropogenic-induced increase in the greenhouse effect. It is supposed, also, that human-induced warming is superimposed on natural cycles of climatic changes. For assessing of possible scenarios of regional and global climatic changes in the 21st century, three major approaches are used by researchers: modeling [4,5]; using proxy data from “natural archives” such as peat, lake, and glacial sediments for investigation of long-term dynamics of climate [6]; and an empirical analysis of modern meteorological data [1]. Presently, an increase in mean annual air temperatures is noted for many regions, according to instrumental observations. The warming is highest in the cryolithozone, where a clear increase in temperature of permafrost is observed [6,7] against the background of a 0.2–0.4 °C general warming of climate in the past decades [1,8]. Some researchers are of the opinion that the degradation of permafrost is happening on a geological scale [5,8], leading to the disturbance of natural processes of mass and energy transportation both in the deep Earth and on the surface [2,9,10]. On the other hand, there are empirical data indicating new frost formation in the zone of discontinuous permafrost in West Siberia [7,11] and suggesting there is no connection between the thickness of seasonal permafrost and emission of carbon [12–14]. At the same time, other investigations demonstrated that organic carbon from frozen peat mounds is especially sensitive to minor climatic change [15]. To better understand the extent and how irreversible the consequences of modern warming of climate are for the arctic and subarctic regions, long-term intervals need to be considered, such as the last interglacial period—the Holocene and Late Quaternary. In this context, multi-proxy high-resolution paleoecological investigations of peat sediments in the zone of discontinuous permafrost are an important source of information. Northern areas of the West Siberian plain with its zones of discontinuous and continuous permafrost and vast peat deposits provide extensive possibilities for such research.

In the north of West Siberia, one of the characteristic and dynamic permafrost geosystems are mounds of perennial heaving (pingo and palsa mires). When studying them, many questions remain unanswered due to the lack of direct long-term observations (geocryological stations only began monitoring in the 1970s) as well as scarcity and limited possibilities of indirect methods to study these features. Such issues include the age of the mounds, the activity of perennial heaving, the effect of anthropogenic disturbances on perennial heaving, etc. [16]. It was found that in the arctic zone of western Siberia, due to an unprecedented melting of permafrost, the threat of methane emissions has increased, and the mires of this region can turn from a net sink of greenhouse gas to a powerful net source [17]. Due to increased thermokarst activity, two contrasting processes are observed here—(a) an increase in the lake surface due to melting of lake coasts, and—a much more important one—(b) a decrease in area or disappearance of lakes due to drainage via the hydrological network [6]. However, large uncertainties remain around the role of thermokarst lakes as a source or sink of greenhouse gas throughout the Holocene [18]. For preservation of

nature of the arctic regions and for responsible exploitation of industrial objects in these areas, information is needed about the dynamics of landscapes and climate both during short-term and long-term periods (decades, centuries, and thousands of years). Such an approach can assess the role of different triggers in modern climate warming. For interpretation of such diverse data, it is important to apply a holistic framework, RHLPS (Environmental–Human–Landscape Feedback and Synergies), suggested by V. Rull [19].

The main research aim of this study is to reveal long-term environmental and climatic changes in the subarctic area of West Siberia using high-resolution paleoecological data from peat–lacustrine sediments extracted from a palsa bog. We present multi-proxy data (spore–pollen, macrofossil, diatom, microcharcoal, radiocarbon, and limited geochemical) to investigate the palsa bog ‘Nadym’ located in the northern taiga zone of West Siberia. This particular site was chosen because of its location in a climatically sensitive geographical subzone in the transition between taiga and forest–tundra, and based on the presence of thick peat deposits in this palsa bog compared to other peat deposits in the area. It is well known that pollen spectra are preserved in the correct stratigraphic order in peat and lake sediments, making them suitable for high-resolution paleo reconstructions. The results are also a valuable contribution to international databases of paleo-pollen and charcoal data, such as PANGAEA (<https://www.pangaea.de/10.1594/PANGAEA.929452> (accessed on 19 December 2023)); the Neotoma Paleoecology Database (<https://www.neotomadb.org/>) (accessed on 19 December 2023).

## 2. Study Area

The study area is located in the north of the West Siberian plain, south of the town Nadym, in the northern taiga (Figure 1). Geographically, this area is unique in many ways. Located near the transition of northern taiga and forest–tundra ecosystems, it presents an extremely variegated vegetation and landscape pattern (Figure 1c). This is due to diversity in lithology, hydrology, and discontinuous spreading of permafrost in soils, and it is also due to a complex history of development of these landscapes in the past, in which repeated climate fluctuations caused significant changes in the water level of the Polar Sea Basin [11]. In general, the territory of the Nadym–Pur interfluvium is a flat, weakly dissected plain of marine and lacustrine–alluvial genesis (absolute height of 60–120 m above sea level) with a predominance of soil-forming rocks of a light texture [20,21]. The study area is located in the zone of discontinuous permafrost, which is mainly confined to hilly and flat-topped peat plateaus as well as to frost mounds [11]. The table of relict permafrost is located at approximately a 100 m depth [22]. About 70% of the study area’s territory is occupied by frozen mires: flat-topped peat plateaus, isolated frost heave mounds (pingos with a shallow layer of peat or without peat), heave plateau areas, and palsa bogs with a thick layer of peat [21]. Frost heave mounds and complexes including palsa bogs are confined to more drained marginal areas of river floodplains. In addition to frozen mires, thawed mires are spread in the Nadym–Pur interfluvium: eutrophic (minerotrophic) lowland mires (2–3%), string–flark mires (1–2%), and raised (bogs) and mesotrophic shrub–sphagnum mires with a tree layer (swamps) occupying not more than 2–3% [6]. Forests and woodlands occupy about 20–30% of the area and are confined to areas where the permafrost disappeared or receded from the surface: in the floodplains and on the terraces of large- and medium-sized rivers, in narrow strips in the floodplains of small rivers, and along the edges of some lakes.

In this research, we carried out a comprehensive paleoecological study of peat and lacustrine deposits of one isolated palsa bog towering 4–6 m above a flat thawed bog (Supplementary Materials, Figures S1 and S2). It is located in the floodplain of the Kheigiyakha River at the ledge of the second floodplain terrace of the Nadym River (65°18′56″ N, 72°52′27″ E) (Figure 1a,b). The plain is characterized by sands with interlayers and lenses of sandy loam and loam. In some places, these sediments are covered by peat deposits [11,23]. The palsa bogs stretch along the floodplain terrace and occupy about 20% of the floodplain thawed mire, represented by marsh sedge–cotton grass–sphagnum plant communities (Supplementary Materials, Figures S1 and S2).

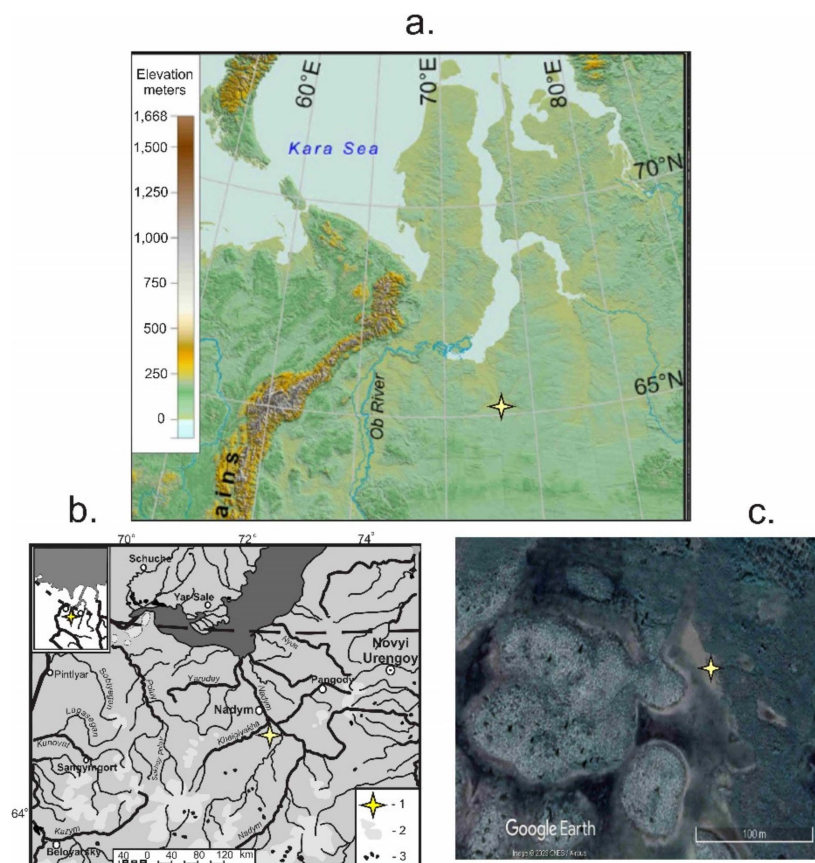


**Figure 1.** Map of study area in the north of West Siberia: (a,b)—the overview maps; (c)—satellite image of mire (data ©2023 Google, CNES, Airbus); 1—location of study point; 2—positive elements of relief formed by remnants of 3-rd fluvial–lacustrine plain according to [11]; 3—lakes.

The tree layer on the palsa mire is represented by single trees of Siberian cedar (*Pinus sibirica* Du Tour) with a trunk diameter of 5–20 cm and a height of 3–15 m (Supplementary Materials, Figure S1). Dwarf birch (*Betula nana* L.), wild rosemary (*Ledum palustre* L.), crowberry (*Empetrum nigrum* L.), and cloudberry (*Rubus chamaemorus* L.) dominate in the understory shrub layer. The ground layer of vegetation cover on the top of the studied palsa bog is dominated by lichens (*Cladonia stellaris* (Opiz) Pouzar & Veda, *Cladonia rangiferina* (L.) Weber ex FHWigg., *Cetraria nivalis* (L.) Kärnefelt & A. Thell., *Cetraria cucullata* (Bellardi) Ach., *Cetraria islandica* (L.) Ach., *Cladonia coccifera* (L.) Willd.) (Supplementary Materials, Figure S2). The mounds of the palsa bog have cracks. Sphagnum mosses (*Sphagnum fuscum* (Schimp.) Klinggr., *Sphagnum rubellum* Wils.) are common in the depressions and on the slopes of the mounds. At the lower levels of the mounds and in thermokarst subsidences, the lichen cover disappears. Shrubs with clumps of *Sphagnum fuscum* dominate here, and in the lowest and moist places, dominance passes to *Sphagnum angustifolium* (Russ.) C. Jens. Thickets of dwarf birch become higher down the slope of the mound, and here it dominates over wild rosemary. In damp areas at the foot of the palsa, *Comarum palustre* L. is abundant, often forming almost pure thickets on a carpet of mosses *Tomenthypnum nitens* (Hedw.) Loeske and *Sphagnum angustifolium*. The mounds of the palsa are surrounded by a thawed damp mire, which is dominated by *Sphagnum lindbergii* Schimp (Supplementary Materials, Figures S1 and S2). Open water is present at some places at the foot of the mounds. Here, one can see thickets of tussock sedge (*Carex* sp.), cotton grass (*Eriophorum polystachyon* L., *Eriophorum vaginatum* L.), reed grass (*Calamagrostis langsdorffii* (Link) Trin., horsetail (*Equisetum hyemale* L.). On the thawed bog, there are plant assemblages of horsetail–sphagnum with *Sphagnum angustifolium*, sedge–bogbeem (*Menyanthes trifoliata*)–horsetail–sphagnum, bogbeem–horsetail–sphagnum, horsetail–sedge–sphagnum

with *Carex rostrata* Stokes and *Carex limosa* L., horsetail–sphagnum. These species assemblages form floating carpets swaying underfoot. Photos of the study site are presented in Supplementary Materials, Figures S1 and S2. Vegetation of mineral uplands on the second terrace above the floodplain is represented by birch–pine forest with common moss–lichen–*Ledum palustre* as the floor cover. Pines 15–16 m high have a diameter of 15–20 cm. The forest is quite sparse with four trees per 100 sq. m. so the forest canopy in these stands is not continuous. Birches 10–8 m high, 4–10 cm in trunk diameter, and 10 trees per 100 sq. m. grow in groups of 2–4 trees. There is a pine undergrowth. The understory shrub layer covers about 60% of the area and is formed by *Ledum palustre* L., *Vaccinium vitis-idaea* L., *Vaccinium uliginosum* L., *Vaccinium myrtillus* L., *Arctous alpina* (L.) Niedenzu. On the forest floor, a moss–lichen cover (*Cladonia stellaris*, *Cladonia rangiferina*, *Cetraria nivalis*, *Cetraria islandica* (L.) Ach., *Peltigera aphthosa* (L.) Willd., *Peltigera canina* (L.) Willd. occupies about 60% of the area. Bryophytes are represented by common mosses, such as *Pleurozium schreberi* (Brid.) Mitt. and *Dicranum congestum* Brid.

In addition to the described forest assemblages, at some distance from the study site, a mixed forest of pine–birch–larch wild rosemary–blueberry with common forest mosses like *Pleurozium schreberi* is present, in which the lichen cover occupies no more than 10–15% of the area, as well as larch–pine and pine–larch sparse forests with lichen ground cover, in which lichens occupy up to 80% of the area. These forests are named ‘white moss forests’ (see Supplementary Materials, Figure S1), which grow on sandy soils.

Slightly to the north, 10–20 km from the study site, on the fifth coastal–marine plain, larch–spruce–cedar blueberry–ledum–common moss paludificated forests are widespread on peat–gley soils. The permafrost rocks usually underly such soils. These forests are distinguished by a higher and denser tree layer of *Larix sibirica* Ledeb., *Picea obovata* Ledeb., and *Pinus sibirica* and a dense understory of *Betula nana* and ericads. The ground cover includes Bryophytes in mixture with lichens (*Peltigera canina*, *Peltigera aphthosa*, *Peltigera canina*, *Cladonia rangiferina*, *Cladonia stellaris*) and occupies no more than 10% coverage.

The climate of the study area is continental, and excessively humid. The average annual air temperature in the study area is  $-6.6\text{ }^{\circ}\text{C}$  (Table 1). The average annual temperature of the frozen ground varies from 0 to  $-2\text{ }^{\circ}\text{C}$ . Snow cover lasts 220–230 days. Most of the precipitation (70–75%) falls in the warm season of the year in the form of low-intensity rains. Stable, strong northerly winds are typical, causing erosion of exposed sandy and peat surfaces, and abrasion of thermokarst lakes [20].

**Table 1.** Climate of Nady (ru.wikipedia.org/wiki/Надым) (accessed on 20 August 2023).

Average Monthly t ( $^{\circ}\text{C}$ )		Average Annual t ( $^{\circ}\text{C}$ )	Annual Precipitation (mm)
January	July		
−24	13.5	−6.6	449

### 3. Materials and Methods

In this work, we used methodology of high-resolution multi-proxy paleoecological studies of lacustrine and peat deposits. The main methods used were as follows: i. In the field—relevés of vegetation and peat outcrops, coring the deposits underneath the palud bog and collecting of subsamples from extracted cores; ii. In the laboratory—collected peat and lacustrine sediments were studied by means of spore–pollen, diatom, macrofossil, and microcharcoal analyses; a peat humification analysis; radiocarbon dating; an elemental analysis; statistical methods.

For paleoecological studies, a core of peat–lacustrine deposits with a thickness of 11 m was taken using a motorized ice drill from the bog surface (Supplemental Materials, Figure S2). The frozen sediments were extracted for 15–20-cm-long core sections, one by one from the top to the bottom of sediments in stratigraphic order. In total, 170 subsamples of a 2 cm thickness were collected from core sections, generally at 2 cm intervals. The intervals increased to 5–10 cm between cores to avoid contamination caused by coring.

Increased intervals were also used for the uppermost accrotelm peat layer and for ice lenses. Subsamples were packed in plastic bags and transported to a laboratory for different analyses. Exact depths for each sample are provided in Supplemental Materials, Table S1. An outcrop of the palsa bog of a 290 cm thickness at 3 m south from the coring point was cleaned (Supplementary Materials, Figure S2), and the texture and color of peat layers were described in the field. The description of lithology was carried out both in the field during coring and later in the laboratory through retrospective series of samples.

Radiocarbon dating was carried out through two methods: the liquid scintillation method (at the Laboratory of Geochronology in Novosibirsk under the supervising of L.A. Orlova) and the method of acceleration mass spectroscopy—AMS laboratory of the Isotope Research Center of the University of Georgia, USA; Isotope Research Laboratory of the National Taiwan University under the supervision of Prof. Hong-Chun Li; 14Chrono Centre at Queens University Belfast, UK; Scottish Universities Environmental Research Centre, UK. For AMS dating, both bulk samples and macrofossils (roots, seeds, pieces of moss twigs) selected under a microscope were used. Realistic (not inverted) radiocarbon dates have been converted from radiocarbon years (before 1950) into calendar years through Calibration curve 3Col\_intcal20.14C in r-space using the CLAM package—<http://cran.r-project.org/package=clam> (accessed on 15 August 2023). The calibrated age of each sample was calculated in the CLAM package using linear interpolation between realistic dates and applied for proxy data [24,25].

For the macrofossil analysis of peat, 116 subsamples with a volume of 2 cm<sup>3</sup> were collected from each peat sample and washed with a 100 µm mesh sieve with running water until the humus color disappeared, according to the method published by [26]. Then, the washed macrofossils were stained with methylene blue, and open slides were prepared for viewing on a microscope at a magnification of 200 times. Macrofossils were identified based on species or group levels using published identification keys [26–31]. The ratio macro-residues of plant species were assessed visually in % over the entire area of the slide of 4–5 cm<sup>2</sup>.

The degree of humification was determined through spectrophotometry of alkaline extracts from standard 1 cm<sup>3</sup> peat samples according to the published protocol of the ACCROTELM method [32,33]. Standard prepared alkaline extracts were scanned on a SHIMADZU UV-240 PC spectrophotometer with transmission at 540 nm. The degree of humification is, thus, expressed in terms of light absorption.

For the spore–pollen analysis, 157 standard volumetric samples of 1 cm<sup>3</sup> were processed through Post’s alkaline method [34], followed by rinsing with distilled water. Mineral contamination was removed through heavy liquid (2.1) treatment. A 300 µm sieve was used to remove large contaminants, and a 10 µm sieve was used to remove small contaminants. Acetolysis and acid treatment were not used, which made it possible to preserve the complexes of diatoms in the lower lake sediments. The spore–pollen analysis of the samples was carried out on a light microscope, Leica, at a magnification of 400 times. To determine palynomorphs, we used the reference literature [29,35–37] and the collection of reference pollen slides stored in the IMCES SB RAS. Exotic pollen was identified with published articles [38–41].

Diatom species, non-pollen palynomorphs (NPPs), and microcharcoal were identified during the pollen analysis in the same samples and slides. For determination of diatoms, we used studies [42,43], and for NPP, we used [44–46].

For a statistical analysis of pollen data, a PCA was performed in R space. For quantitative reconstructions of past mean annual temperature, mean January temperature, and mean July temperature (in °C), we used the information–statistical method of V.A. Klimanov [47]. The calculations were carried out using the Excel program and the R space. Diagrams were created using Tilia software [48]. A cluster analysis of paleopalynological data was performed in Tilia, to confirm palynological zones. For the cluster analysis, only pollen of dryland vegetation has been used.

## 4. Results

### 4.1. Lithology

Studied deposits of the palsa bog were represented from top to bottom as follows: 0–42 cm thawed peat; 42–604 cm frozen peat; 604–909 cm frozen lacustrine deposits (gyttja); 909–1076 cm frozen red-brown sediments with a granulate texture (Table 2). On the cleaned 290-cm-thick outcrop of the palsa bog, the peat layers varied in color from ochre in the upper part of the section to brown in the lower part (Table 2, Supplementary Materials, Figure S2). The structure of the frozen peat section was represented by layers of peat with parallel stratification and layers of peat with highly cryoturbated layering (Supplementary Materials, Figure S2). Ice veins of horizontal or slightly inclined bedding with a thickness of one to several centimeters existed in the peat and lacustrine deposits. Lacustrine sediments mainly consisted of gray gyttja and were strongly icy. From the depth of 885 cm and below 916 cm (see Table 2), sediments acquire a red-brown color and crumbling granulate texture formed by granules (or nodules) with a diameter of 0.3–1 mm and brown color (Figure 2). The elemental analysis of these granules performed using a scanning microscope (Figure 2d) revealed a presence of mainly iron in them. In addition, rounded quartz particles were found (Figure 2a–c).

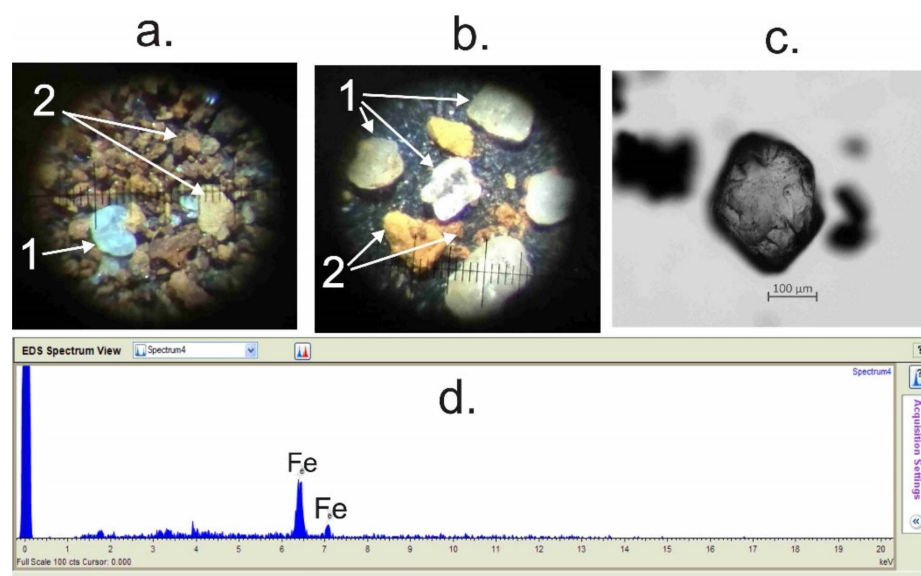


**Figure 2.** Microscopic texture of the bottom (940–947 cm) sediments in the Nadyim sediment core and its elemental composition: (a–c)—microscope images with 20× magnification. 1—rounded quartz particles; 2—iron–argillaceous concretions (grains); (d)—EDS spectral data.

### 4.2. Radiocarbon Dating

For the Nadyim sediment section, 21 radiocarbon dates were obtained (see Table 3). The liquid scintillation method (LSM) was used to date peat samples at the Radiocarbon Laboratory of the Institute of Geology and Mineralogy in Novosibirsk under the supervision of L.A. Orlova. The AMS method was used to date a number of samples from lake sediments containing very little carbon and three uppermost samples of weakly decomposed peat. All LSM data are in the correct sequence. Among the AMS dates, we were able to use only four dates for the depth–age model. Three of them are from peat sediments (depths 23–25, 27–29, and 601–610 cm) and one date is from lake sediments at the depth of 789–791 cm. The remaining 10 AMS dates performed on bulk lake samples and on small macrofossils collected from lacustrine samples turned out to be too young compared to surrounding sediments or failed during the analysis. Those dates are marked with asterisks in Table 3 and were not included in the depth–age model (Figure 3).

Table 2. Core stratigraphy.

Depth in the Section (in cm) and Number of Subsamples (in comas)	Type of Sediment	Color	Texture
0–42 (5)	Peat	Red-ochre	Thawed, weakly decomposed (by description of outcrop and drilled core)
50–70 (5)		Dark brown with black layers	Frozen with even layering (by description of outcrop and drilled core)
70–125 (9)		Black-brown	Frozen, heavily cryoturbated (by description of outcrop and drilled core n)
125–210 (18)			
210–225 (3)		Light brown	Frozen with parallel layering (by description of outcrop and drilled core)
225–260 (9)		Brown-mottled peat with dark and light interlayers	
260–290 (6)		Brown-mottled peat with large black horsetail macrofossils	Frozen, heavily cryoturbated with ice schlieren (by description of outcrop and drilled core)
290–604 (53)		Brown	Frozen (from this depth and deeper, descriptions were made by drilled core samples)
604–634 (6)	Peaty gyttja	Brown	Homogeneous with small macrofossils, very icy
634–648 (2)		Brown	Homogeneous with larger macrofossils
650–652 (1)		Light brown	Homogeneous with small macrofossils
655–689 (7)	Gyttja	Brown-gray	Homogeneous, very icy
694–696 (1)			Homogeneous, less icy
701–724 (2)		Gray	Homogeneous, very icy
728–730 (1)		Dark gray	Homogeneous, less icy
735–750 (3)		Gray	Homogeneous, very icy
755–757 (1)		Ice	Transparent
770–779 (1)	Diatom gyttja	Gray	Homogeneous with inclusions of small macrofossils
782–798 (3)			Homogeneous with inclusions of small fibrous macrofossils, icy
801–831 (5)			Homogeneous
836–845 (1)			Homogeneous with inclusions of macrofossils, very icy
845–864 (3)			Homogeneous, very icy
869–880 (2)			Homogeneous, very icy
880–891 (4)	Gyttja	Gray-brown	Homogeneous with inclusions of plant macrofossils, very icy
896–909 (2)	Gyttja	Gray-brown	Homogeneous with whitish granules
916–968 (7)	Granulate sediments	Red-brown with light specks	Variegated plastic with iron–clay granules
973–989 (3)		Dark red-brown	Homogeneous, icy
991–1000 (2)		Dark red-brown with light specks	Homogeneous with iron–clay granules, highly icy
1005–1007 (1)		Black-brown	
1012–1034 (2)		Brown-gray with light and dark granules	
1041–1053 (1)		Brown with light granules	
1058–1076 (1)		Gray-brown	

Colors in the table mark different sediment layers: ocher brown shades—peat; gray shades—gyttja; red-brown shades—ancient gyttja.

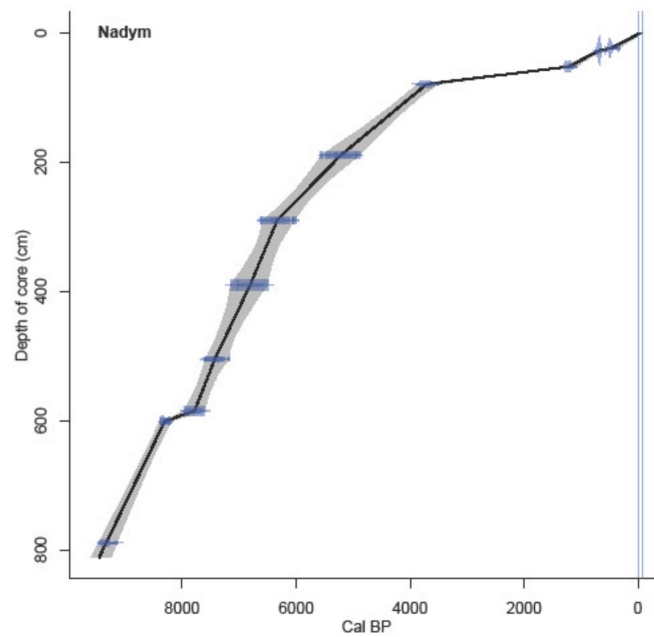


Figure 3. Depth–age model constructed in CLAM [23].

Table 3. Radiocarbon dates for Nadyim lacustrine–peat sediments.

Depth (cm)	Age C14 (yr BP)	Calibrated Age ** (cal. a BP)	Laboratory №	Method	Material
23–25	422 ± 45	529–425	SUERC-48843	AMS	Peat bulk
27–29	740 ± 45	732–644	SUERC-48844	AMS	Peat bulk
2–54	1288 ± 45	1236–1174	UBA-44701	AMS	Peat bulk
79–82	3450 ± 65	3883–3560	SOAN-8379	LSA	Peat bulk
189–200	4560 ± 120	5478–4953	SOAN-8380	LSA	Peat bulk
290–300	5540 ± 115	6564–6171	SOAN-8381	LSA	Peat bulk
390–406	5960 ± 125	7031–6498	SOAN-8382	LSA	Peat bulk
505–512	6530 ± 110	7597–7255	SOAN-8383	LSA	Peat bulk
585–598	6945 ± 110	7964–7604	SOAN-8384	LSA	Peat bulk
601–610	7503 ± 47	8388–8276	NTU AMS-3485	AMS	Peat bulk
681–683	7173 ± 122 *		NTU AMS-3487	AMS	Gyttja bulk
728–730	5365 ± 31 *		NTU AMS-3486	AMS	Gyttja bulk
789–791	8321 ± 45	9463–9249	NSK00474	AMS	Gyttja bulk
829–831	7110 ± 60 *		NTUAMS-3777	AMS	Gyttja bulk
882–884	Failed *		UBA-44702	AMS	Macrofossils
961–962	2048 ± 35 *		UBA-44703	AMS	Macrofossils
966–968	2048 ± 35 *		UBA-44703	AMS	Macrofossils
1000–1007	Failed *		UBA-44704	AMS	Macrofossils
1063–1076	Modern *		UBA-44705	AMS	Macrofossils
1074–1076	Modern *		NTUAMS-3478	AMS	Gyttja bulk
1074–1076	Failed *		UBA-44706	AMS	Macrofossils

\* Radiocarbon dates not used in depth–age model. \*\* Calibration was made in CLAM program based on 2Col\_intcal20.14C calibration curve [24].

#### 4.3. Macrofossil and Humification Data

Results of the macrofossil analysis of 116 samples from the 630-cm-thick peat sediments are presented in Figure 4. Mosses dominated the plant remains, but other mire plants were also present. Five major types of peat were distinguished based on remains of different mire plants: 1. At the base of the peat sediments (630–580 cm), there is a layer of peat formed by remains of cattail (*Typha*), submerged aquatic plants (*Nuphar*, *Myriophyllum*), and littoral aquatic plants. 2. At the depth 580–450 cm, the mire deposits are formed by eutrophic types of peat. Remains of common mosses (*Hypnum*) dominate first. Above the layer of pure *Hypnum* peat, there is a layer of herbal horsetail–sedge peat (520–500 cm). Next, eutrophic bogmosses (*Sphagnum*) dominated: *Sphagnum teres* (Schimp) Aogstr. ex Harm and *Sphagnum riparium* Aungstr. Herbaceous peat has a high degree of humification, which considerably decreases with transition to sphagnum peat. It is worth it to note a sudden change in plant remains forming the peat layers. 3. The sphagnum peat of a meso-oligotrophic origin was deposited at the depth 450–300 cm. It starts with a thick layer of meso-oligotrophic *Sphagnum angustifolium* peat, which later alternates with layers of *Sphagnum jensenii* H. Lindb. and common moss (Hypnaceae) peat. In general, a low degree of humification characterizes this peat. 4. At the depth 300–170 cm, the peat is formed through alternation of layers of cotton grass (*Eryophorum*), bogmoss (*Sphagnum*), and common moss peat. These are plants indicative of oligotrophic conditions, but with contrasting hydrologic demands. The degree of humification increased and showed sharp changes in this section. 5. At the depth from 170 cm to the surface of the mire, the thick strata of peat are formed mostly by remains of more xerophytic oligotrophic *Sphagnum* species—*Sphagnum fuscum* (Schimp) Klingr. An interlayer of *Carex juncella* (Fries) Th. Fries. together with cotton grass (*Eryophorum*) and dwarf shrubs followed by remains of two *Sphagnum* species (*Sphagnum jensenii* and *Sphagnum magellanicum* Brid.) are found at the depth of 52–54 cm. After that, *Sphagnum fuscum* peat dominates again near the surface of the mire. Maximum peat humification was found at a depth of 75–60 cm.

#### 4.4. Spore–Pollen and Microcharcoal Data

The method of the spore–pollen analysis was used to study 157 samples with a step of 2–5 cm. Depending on the rate of peat (and ice) accumulation in different periods, the temporal resolution between samples ranged from 470 years in the uppermost samples to 12 years in the more ancient sediments. The results of the spore–pollen analysis of lake-peat deposits of the Nadym section are presented in a diagram (Figure 5). The cluster analysis of paleopalynological data performed in the Tilia software package divided the spore–pollen diagram into four local pollen zones (LPZs) based on the dynamics of pollen of trees, shrubs and grasses, excluding *Carex*, exotic pollen, and NPP. Although the latter components were not taken into account in the cluster analysis, nevertheless, there is a clear confinement of certain groups of NPP (diatoms) and redeposited pollen of exotics [38,39,42] mainly to LPZ-2. The description of the local pollen zones presented from the bottom to the top from more ancient deposits to younger ones is as follows:

1. LPZ-1 of downy birch (*Betula pubescens*), grasses (Poaceae), spruce (*Picea*), and Siberian pine (*Pinus sibirica*) distinguished depths 1040–850 cm. In general, this pollen zone covers bottom red-brown deposits in which radiocarbon dating was unsuccessful; therefore, the age of this zone is unknown. The pollen zone is not uniform in the ratio of pollen components, but the most characteristic feature of this pollen zone is the maximum abundance of downy birch pollen (*Betula pubescens*) and pollen of grasses (Poaceae). In addition, there is quite a lot of Siberian pine (*Pinus sibirica*) and spruce (*Picea*) pollen in LPZ-1. The abundance of pollen of larch (*Larix*), silver birch (*Betula pendula*), and Scots pine (*Pinus sylvestris*) varies greatly. It is possible to divide LPZ-1 into three subzones according to the abundance of the last three components. There is relatively little pollen from dwarf birch (*Betula nana*) and wormwood (*Artemisia*) in this zone. Microcharcoal is present in small amounts.

2. LPZ-2 of spruce, larch, Siberian pine, and wormwood (*Artemisia*) was recognized at the depth 850–650 cm in gray lacustrine sediments. The reliable radiocarbon date for lacustrine sediments is for a depth of 789–791 cm (Table 3), which allows the LPZ-2 to be dated c. 9800 to 8600 cal. a BP. This pollen zone is characterized by the dominance of spruce, Siberian cedar, and larch pollen. Pollen of Scots pine and silver birch is present at a lower abundance. The abundance of downy birch pollen (*Betula alba*) is significantly reduced in comparison with the previous pollen zone, whereas the abundance of willow (*Salix*) and spirea (*Spiraea*) pollen increased. Of the herbal group, pollen of grasses, wormwood, and haze (*Chenopodiaceae*) dominate. The abundance of pollen of *Urticaceae*, *Lycopodium dubium*, *Lycopodium clavatum*, *Monoletes*, and *Trilete* fern spores also increased, as did spores of common mosses (*Bryales*). Microcharcoal particles are most abundant in this zone. A characteristic feature of this LPZ is an abundance and diversity of exotic Neogene and Paleogene pollen and spores (*Tilia*, *Pterocarya*, *Carya*, *Mirica*, *Comptonia*, *Quercus*, *Tsuga*, *Trudopollis*, and *Ceratopteris* identified according to [38,39,41]; see Figure 6).

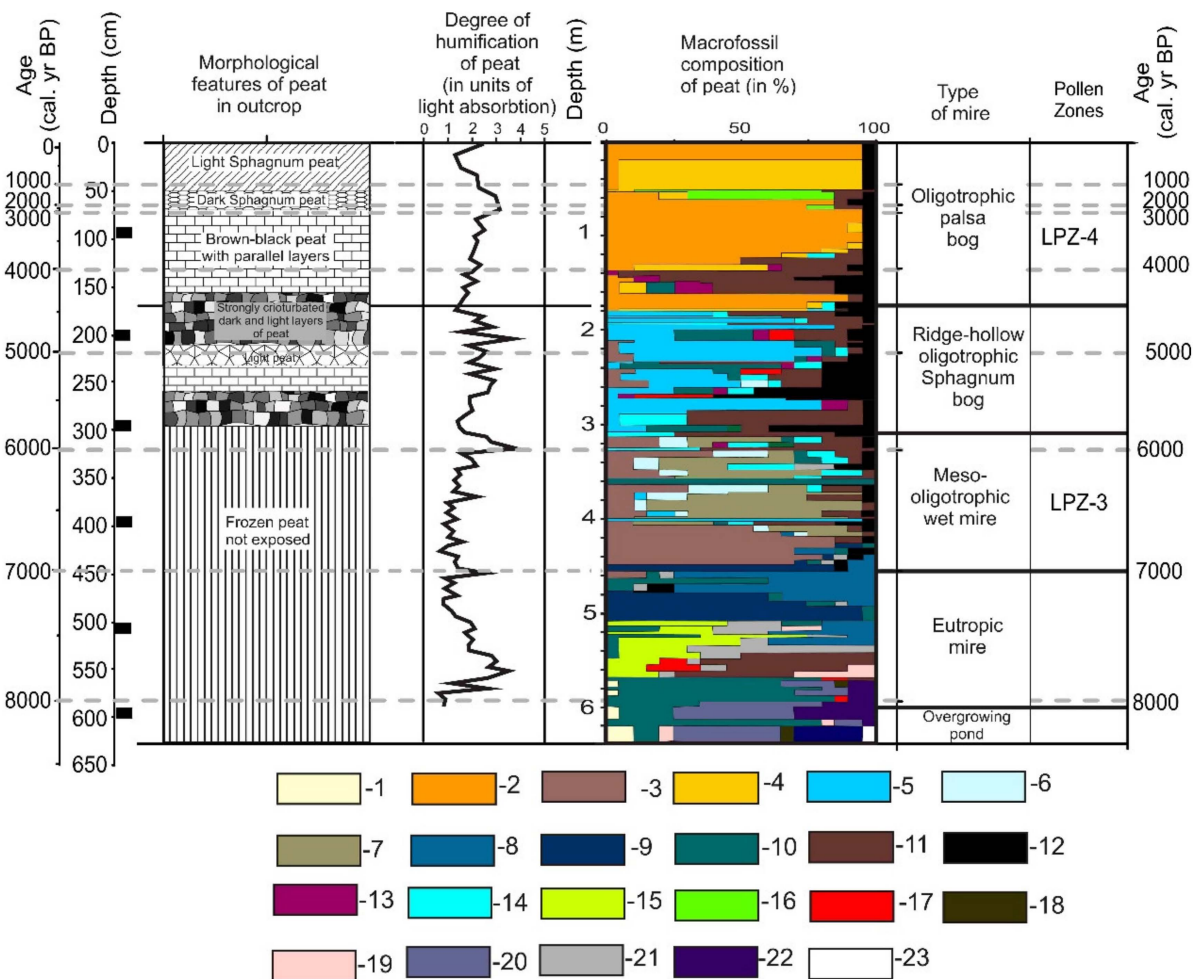


**Figure 4.** Lithology, macrofossil composition, and degree of humification of peat deposits in Nadym section. Conventional marks for plant remains in peat: 1—*Sphagnum* sp.; 2—*Sphagnum fuscum*; 3—*Sphagnum angustifolium*; 4—*Sphagnum magellanicum*; 5—*Sphagnum balticum*; 6—*Sphagnum majus*; 7—*Sphagnum jensenii*; 8—*Sphagnum riparium*; 9—*Sphagnum teres*; 10—Hypnaceae; 11—*Eryophorum*; 12—shrubs; 13—*Sheuchzeria*; 14—*Carex lasiocarpa*; 15—*Carex cespitosa*; 16—*Carex juncella*; 17—*Menyanthes*; 18—*Myriophyllum*; 19—*Betula nana*; 20—*Tipha*; 21—*Equisetum*; 22—water plants; 23—*Nuphar*.

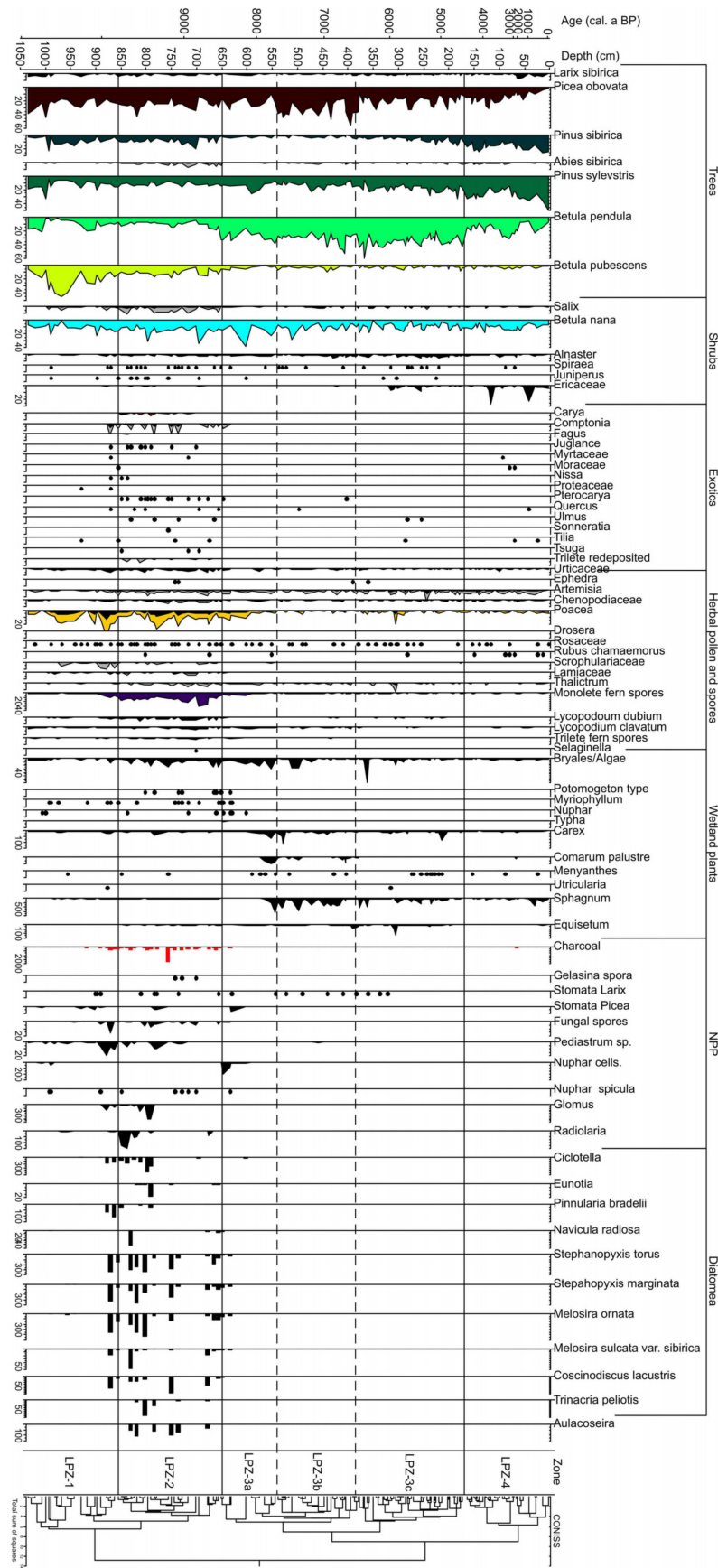


**Figure 5.** Overview of spore–pollen, NPPs, and diatoms (percentages calculated from sum of all pollen and spores except Bryales/Algae and *Sphagnum*).

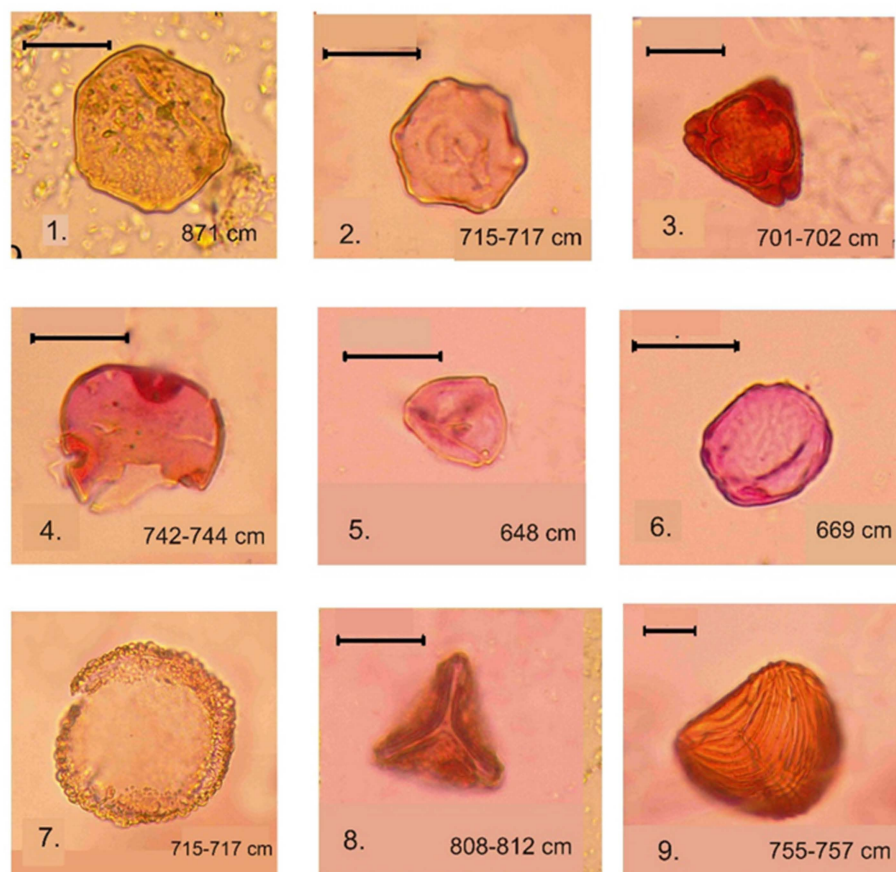


**Figure 6.** Exotic redeposited pollen: 1—*Juglance*; 2—*Carya*; 3—*Trudopollis arecta* (according to [49]); 4—*Tilia*; 5—*Comptonia*; 6—*Ulmus*; 7—*Tsuga*; 8, 9—spore of exotic fern (*Ceratopteris*). Scale bar represents 20  $\mu$ m. Identified according to [38–41].

In addition, the abundance of fragments of diatoms typical for both freshwater and brackish water are confined to LPZ-2 (identified according to [42,43]; see Figure 7). It is noteworthy that these components are not found in the previous pollen zone and disappear in the next pollen zone. Among other NPP present are spores of fungi, *Glomus*, and *Gelasina*. Spruce and larch stomata are consistently found in this LPZ.

3. LPZ-3 of spruce and silver birch pollen is found at the depth of 650–150 cm and covers layers of peaty gyttja and peat. The estimated age of the pollen zone according to the depth–age model is c. 8500–4300 cal. a BP. On the whole, the entire LPZ-3 is characterized by the dominance of the pollen of silver birch (*Betula pendula*) with a smaller proportion of the pollen of Scots pine and spruce and a very small proportion of Siberian pine (*Pinus sibirica*) pollen. Alder (*Alnaster*) is typically present and the abundance of dwarf birch pollen (*Betula nana*) gradually decreases toward the end of the zone. There is very little pollen from downy birch and wormwood. Components of local pollen are presented first by *Myriophyllum*, *Nuphar*, *Tipha*, and *Menyanthes*, then by *Carex* and Bryales, and, finally, by *Sphagnum* spores. Pollen of ericoid shrubs (Ericaceae) appears from about 316 cm (5980 cal. a BP).

LPZ-4 includes Siberian cedar, Scots pine, and larch pollen. This pollen zone covers the upper 150 cm of oligotrophic peat, deposited during the last 4300 years. The dominance of Siberian pine and Scots pine pollen is a characteristic feature of the pollen zone. The abundance of silver birch pollen cyclically varies by depth, showing two maxima and two minima. The abundance of spruce pollen has been progressively decreasing toward the present, while larch pollen is increasing. The abundance of dwarf birch and wormwood pollen slightly increased compared to the previous pollen zone. Two large maxima of the

pollen of ericoid shrubs and one large burst in the abundance of *Sphagnum* spores are noted, together with a slight increase in the abundance of microcharcoal in this zone. Careful examination of the upper part of the deposits at the depth of 68–74 cm (2751–3220 cal. a BP) indicates that these two samples contain a maximum of detritus, roots, hyphae, amorphous organic matter, and many rounded black-brown glomeruli, suggesting contamination with lichen remains.

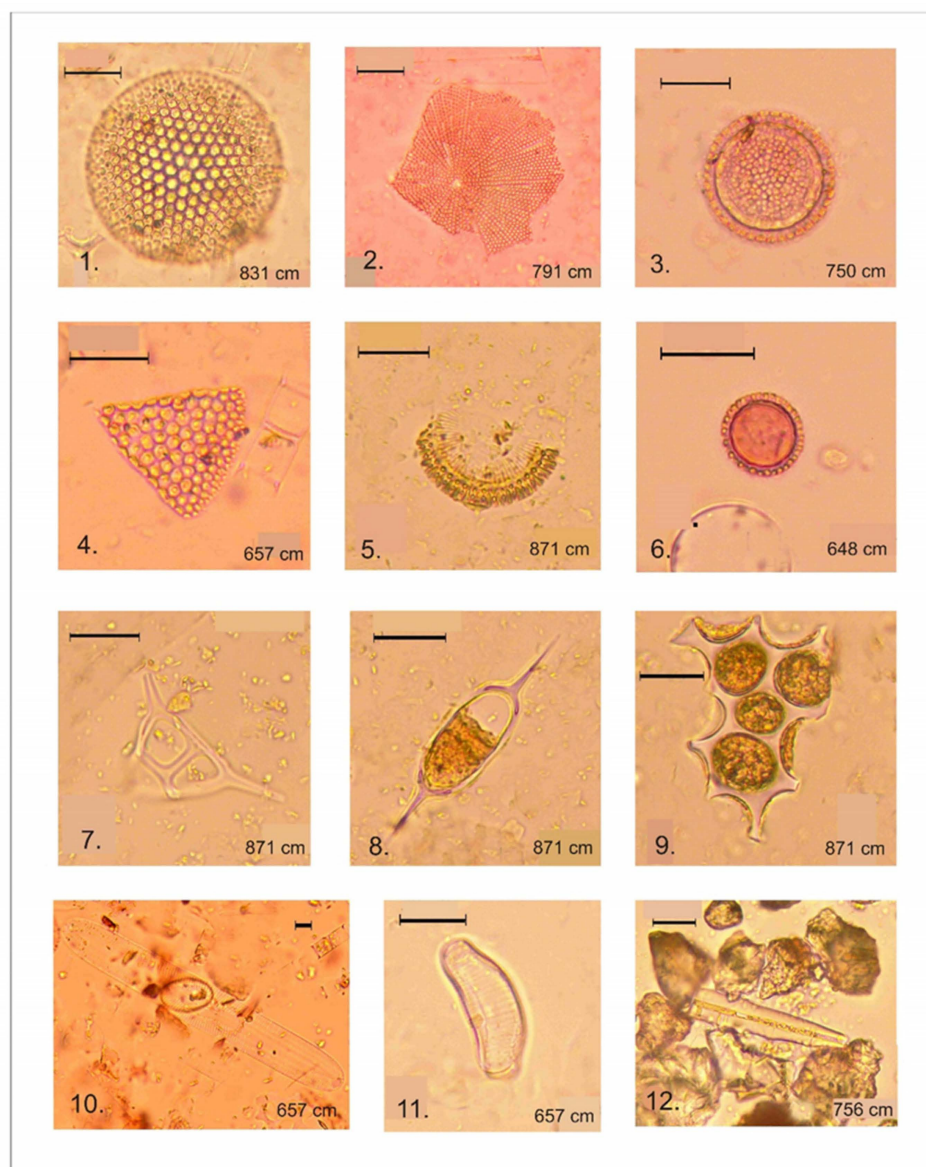


**Figure 7.** Diatom frustules and other NPPs: 1—*Stephanopyxis marginata*; 2—*Coscinodiscus lacustris*; 3—*Stephanopyxis torens*; 4—*Trinacria peliotis*; 5—*Melosira sulcata* var. *sibirica*; 6—*Melosira ornata*; 7–8—*Silicoflagellatophycidae*; 9—*Radiolaria*; 10—*Pinnularia bradelii*; 11—*Eunotia exigua*; 12—spicula. Scale bar represents 20  $\mu\text{m}$ . Identified according to [42,43].

#### 4.5. Non-Pollen Palynomorph (NPP) Data

As mentioned in Section 3, non-pollen palynomorphs (NPPs) were also counted during the spore–pollen analysis. They are presented in Figure 5 in absolute counts. In sediments deeper than 900 cm, typical NPPs are spicules and basal cells of the water lily *Nuphar* and the algae *Pediastrum*, as well as findings of stomatal cells from spruce, larch, and cedar [46]. The abundance of microcharcoal is minimal in the lowest samples and slightly increases toward the top of brown sediments. Numerous NPPs are found in the

lacustrine sediments underlying the peat sediments at the depth of 850–650 cm (pollen zone LPZ-2). Spicules of the floating macrophyte *Nuphar* are often found here, along with an abundance of *Nuphar* basal cells. The types of diatoms are diverse in the sediments of this depth. In most cases, the diatom frustules are damaged and fragmented. Among diatoms (Figure 7), there are both freshwater [43] and brackish water [42,43] species: *Eunotia exigua*, *Melosira ornata*, *Melosira sulcata* var. *sibirica* Grum., *Pinnularia brandelii*, *Navicula radiosa*, *Stephanopyxis turris* var. *arctica* Grum., *Stephanopyxis marginata* Grum., *Coscinodiscus lacustris*, *Aulacoseira alpigena*, *Trinacria piliotis* var. *josephina*. The same sediments contain fragments of radiolarians, spores of fungi, including the soil fungus *Glomus*, and the microscopic algae *Pediastrum*. The 850–650 cm layer is characterized by an increased amount of microcharcoal.

In the peat deposits at the depth of 591–0 cm, several types of testate amoebae are found: *Archerella flavum*, *Archerella wrightianum*, *Assulina muscorum*, *Assuluna seminulum*, *Arcella* sp. (*A. artocrea*, *A. arenaria*), *Cyclopyxis eurystoma*, *Bullinaria indica* v. minor, *Diffugia bacillifera*, *Diffugia globulosa*. Other NPPs, typical for oligotrophic bogs, were constantly encountered, *Microbotus amhiguus*, *Tiletia*, *Rotatoria*, *Callidina angustilobus*, *Rhabdocoela*, metasternums of Coleoptera, and Chironomidae [44,45], but excluded from Figure 5 to improve readability. Generally, peat samples contained a very small number of microcharcoal particles. The abundance of charcoal slightly increased only from the depth of 150 cm and upper depths (from the age of c. 4200 cal. a BP to present).

## 5. Discussion

### 5.1. Interpretation of Radiocarbon Dating

We assume that the sequence is in correct stratigraphic order, despite several radiocarbon dates that appear too young for their stratigraphic position (Table 3). A likely explanation for the young radiocarbon dates in the deposits underlying the peat sediments is that contamination with younger carbon happened during the coring process. From lacustrine deposits, we used only one radiocarbon date,  $8321 \pm 45$ , for the depth 789–791 cm for the depth–age model. The four other radiocarbon dates for lacustrine deposits appear contaminated by younger carbon. Failure of AMS dating of the deepest red-brown granulate samples is likely caused by their very low carbon content. Another possible explanation is that sediments deeper than 880 cm were unsuccessfully dated because they contain carbon that is too old for dating with radiocarbon. Similar unsuccessful (modern or failed) AMS dates for these sediments were obtained in two different laboratories (the Radiocarbon Laboratory of National Taiwan University (NTUAMS) and the 14Chrono Centre at Queens University Belfast. Unsuccessful radiocarbon dates of low sediments of the Nadym section did not allow us to date these sediments, and to make retrospective interpretation of pollen data of this stratum.

### 5.2. Principal Component Analysis of Nadym Pollen Data and Its Interpretation

We analyzed pollen spectra of the Nadym section using a Principal Component Analysis (PCA) to identify the nature of pollen zones and the relationship of pollen spectrum components with each other and with the history of landscape development. For this analysis, we did not use data on the abundance of spores, since these local components in individual samples give sharp bursts of abundance, which can distort the overall picture of vegetation cover dynamics. The results of the PCA analysis are shown in Figure 8. Conventional marks were assigned to the samples of each pollen zone (see right low corner of the figure). The analysis showed that axes 1 and 2 explain 12.9% and 7.5%, respectively, of the variance in the pollen data. The Principal Component Analysis clearly separated pollen spectra of each pollen zone in four pollen assemblages, which reflect specific stages in the development of landscape and vegetation of the Nadym area.

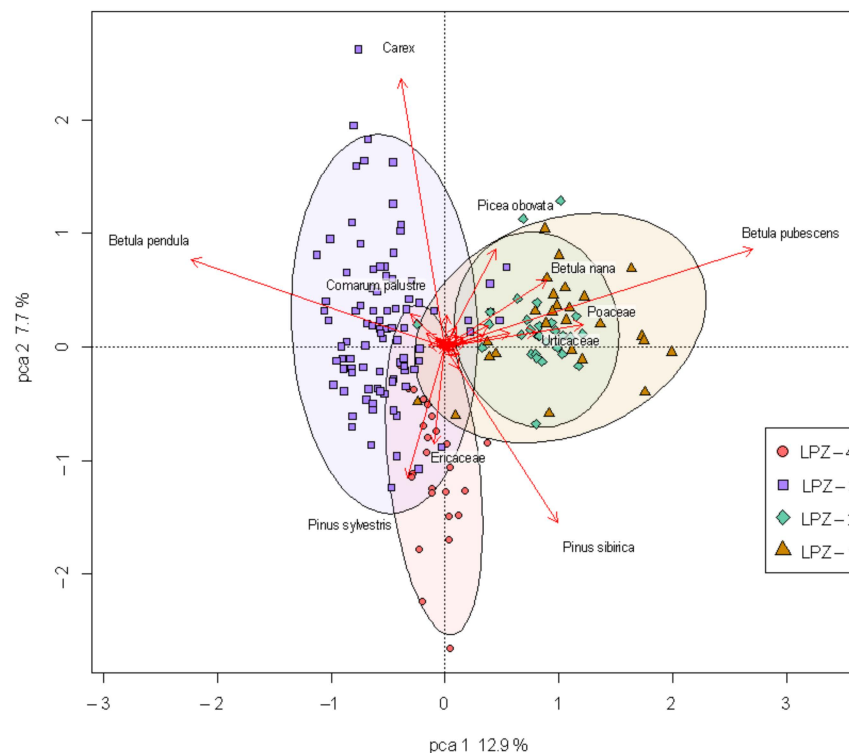


**Figure 8.** PCA plot of pollen data. LPZs—local pollen zones (according to Figure 5).

1. The first stage in landscape development is based on samples from deposits at a 1034–850 cm depth (LPZ-1) (non-defined age). *Betula pubescens* is the dominant component of this pollen assemblage. It is also characterized by a large species diversity of herbs (Poaceae, Apiaceae, Scrophulariaceae, *Thalictrum*, Onagraceae, Rosaceae, *Galium*, *Potentilla*, Lamiaceae), positively correlated with each other and with such tree species as *Betula pubescens*, *Picea*, *Abies*. Pollen of xerophytic species *Artemisia* and Chenopodiaceae and pollen of aquatic plants *Nuphar*, *Myriophyllum*, and *Typha* are also associated with this period. Such pollen spectra reflect the dominance of birch–coniferous forests and lakes surrounded by thickets of willows and cattail in landscapes. Different water macrophytes (*Nuphar*, *Myriophyllum*) thrived in the lake. However, the same pollen assemblage indicates a presence of open dry tundra based on the abundance of xerophyte and dwarf birch pollen (*Betula nana*, *Artemisia*, Poaceae). The large ecological diversity of the pollen components probably reflects the mixed nature of the pollen assemblages at these depths, which include pollen from both glacial and interglacial landscapes. Pollen complexes of this stage are not in concert with literature data for this area [6], and the Early Holocene age of this stage is not supported through realistic radiocarbon dating. Thus, we assume that the first pollen assemblage can reflect ancient deposits of an (indetermined) Quaternary interstadial period. An alternative hypothesis could be that very warm and wet climatic conditions existed during the Late Glacial and Early Holocene time in northern West Siberia, which is inconsistent with previously published data. Both hypotheses, however, must be tested through additional research in the north of West Siberia.
2. The second stage in the development of landscape represented by pollen complexes of LPZ-2. In this stage, the xerophytic species of *Artemisia* and Chenopodiaceae and pollen shrub birch (*Betula nana*) together with aquatic and wetland plants—*Typha* and *Myriophyllum*—are the most important. The radiocarbon dating of LPZ-2 is more realistic, covering c. 9800–8400 cal. a BP of the Early Holocene. The spectra are enriched by diatoms, exotic pollen, and NPPs (charcoal, *Glomus*, fungal spores), indicating intensive erosion of soil material into the lake basin. We assume that during the Early Holocene, the north part of West Siberia experienced increasingly

wet conditions that caused redeposition of exotic pollen by flowing surface waters. Exotic pollen includes both very old Neogene pollen [40] and pollen redeposited from Quaternary interstadials. Thus, the pollen spectra of LPZ-2 became enriched in pollen of *Picea* and *Pinus*. Possibly, only pollen of Poaceae, Chenopodiaceae, *Betula nana*, and *Lycopodium* spores originates from Early Holocene vegetation. In general, however, the pollen spectra of this part of the sequence are mostly redeposited, and can be used for reconstruction of real vegetation of that time with great caution. The overlap of LPZ-1 and LPZ-2 in Figure 8 also visualizes the hypothesis about the mixed origin of pollen in LPZ-2.

3. The third stage in the development of landscape is represented by LPZ-3. *Betula pendula* and *Carex* are taxa-abundant in LPZ-3, and plotted on the left side of the PCA biplot (Figure 8). During this stage, c. 8200–6000 cal. a BP, the landscapes of Nadym began to be dominated by birch swamp forests, combined with thawed sedge mires in eutrophic and mesotrophic states. Thickets of alder (*Alnaster*), whitehead (*Filipendula*), and burnet (*Sanguisorba*) were common at the margins of the mires. Sedges (*Carex*) alternated with areas of *Menyanthes* and *Comarum palustre* dominated the swamps. The pollen of all these species positively correlates with each other in the PCA biplot (Figure 8). We argue that these pollen complexes have an autochthonous origin and represent the real vegetation types that existed in the study area during the middle Holocene. It reflects spreading of birch forests and complex meso-oligotrophic bogs with trefoil (*Menyanthes trifoliata*) and scheuchzeria (*Scheuchzeria palustris*) thriving in wet hollows and cloudberries (*Rubus chamaemorus*) growing on ridges.
4. The fourth stage in landscape development is reflected in LPZ-4. Typical taxa for LPZ-4 are located in the lower part of the PCA biplot. The leading pollen components are *Pinus sylvestris* and Ericaceae. They reflect dominance of pine forests and oligotrophic frozen peatlands (palsa bogs) in the landscape of Nadym. In these assemblages, pollen of *Pinus sylvestris*, *Pinus sibirica*, *Larix sibirica*, Ericaceae, and *Drosera* is positively correlated with each other.

### 5.3. Interpretation of Macrofossil Data

A detailed macrofossil analysis of peat made it possible to reconstruct the succession of the peat-generating plant communities of the mire for the entire period of peat accumulation, which, according to radiocarbon dates, continued for the past c. 8400 years. The chronology of these changes is based on six radiocarbon dates (Table 3). The AMS radiocarbon date from the depth of 52–54 cm is rather old,  $1288 \pm 45$  years (Table 3), which indicates a sharp slowdown (or termination) of peat accumulation in the past millennia (Figure 3). Macrofossil data reveal a picture of autogenic development of the mire, which arose through overgrowing and infilling of a floodplain lake. Macrofossil data (Figure 4) reveal five autogenic stages in the development of the mire (in chronological order):

1. The stage of an overgrowing shallow lake (650–590 cm, 8400–8000 cal. a BP) was where aquatic macrophytes—*Nuphar* and *Myriophyllum*—thrived. Cattail (*Typha*) and dwarf birch (*Betula nana*) grew on the banks of the lake.
2. A eutrophic (minerotrophic) mire was formed through the lake infilling process, c. 8000 cal. a BP. It existed from about 8000 to 7000 cal. a BP. In the peat core, this stage can be traced at the depth of 600–450 cm. It is represented first by layers of common moss (*Hypnum*) and cotton grass (*Eriophorum*), then by horsetail–sedge peat, and finally by pure minerotrophic *Sphagnum* peat. At the depth of 510 cm, the last herb–grass mire plant assemblage was replaced by a purely *Sphagnum* assemblage of the eutrophic (minerotrophic) hydrophytic *Sphagnum* species—*Sphagnum teres*—which was later replaced by the mesotrophic hydrophytic species—*Sphagnum riparium*. It reflects a gradual autogenic successional pathway of mire development from wet common moss carpets (*Hypnum*) with cotton grass tussocks to a wet horsetail–sedge mire and finally to a minerotrophic sphagnum mire. This succession reflects nutrient impoverishment as 140 cm of peat accumulates. Herbaceous peat has a high degree of

humification, which decreased considerably with transition to *Sphagnum* peat. One can mention a sharp change in the dominance of some plant macrofossils compared to others.

3. As peat accumulated, the mire became mesotrophic around c. 7000 cal. a BP (160 cm) and gradually transitioned to a meso-oligotrophic stage. Based on the ecology of plant species, the mire was thawed at this stage and heavily waterlogged (lawns of hydrophytic bog mosses and common mosses). The mesotrophic wet moss stage continued until c. 5800 cal. a BP (~1200 years between 450 and 300 cm). The peat was composed by *Sphagnum* mosses preferring meso-oligotrophic ecology. In the lower part of the stratum, there is a peat layer formed by the mesotrophic hydrophytic moss *Sphagnum riparium*. Above it lies a rather thick layer of peat formed by the meso-oligotrophic hydrophytic *Sphagnum angustifolium*. Above it, there is a layer of peat formed by *Sphagnum jensenii*, a species growing in transit spring mires and in wet hollows of oligotrophic string-flark patterned bogs. All of these plant species grow well in thawed waterlogged mires. At the end of the meso-oligotrophic stage, the species of cotton grass (*Eryophorum* sp.) and marsh dwarf shrubs increasingly spread on the mire. Heterogeneous microtopography of the string-flark pattern probably formed at the end of this stage. Cotton grass-dwarf shrub assemblages grow on the ridges and hydrophilic mosses in the hollows.
4. After c. 5800 cal. a BP, the mire passed into the oligotrophic stage of development with the oligotrophic ridge-hollow patterns, which lasted for about 1300 years until c. 4400 cal. a BP (300–170 cm). The sequence is composed of alternating layers of cotton grass, *Sphagnum*, and common moss (*Hypnum*) peat. The contrasting ecology of plants, forming sharply alternating independent layers of peat, provides evidence for the existence of small-scale ridge-hollow surface patterns on the bog. Humid hollows were occupied by hydrophytic *Sphagnum balticum* (Russ.) Russ. Ex C. Jens, and ridges were covered by cotton grass-shrub cover and common moss *Straminergon stramineum* Dicks. Ex Rid.
5. At the depth of 180 cm in the peat deposit, there is an abrupt change in peat formed by hydrophytic oligotrophic species *Sphagnum balticum* to the peat of more xerophytic oligotrophic species—*Sphagnum fuscum*. This change took place at c. 4500 cal. a BP. Currently, such plant communities dominate the vegetation cover of low frozen peat mounds (palsa bogs). An abrupt change probably marks the beginning of frost heaving in the bog. Epigenic freezing of a previously thawed bog caused strong cryoturbation in the moisture-saturated peat layers (see Table 2, Figure 4), deposited earlier in the stage of the ridge-hollow patterned bog. An interlayer of peat formed by *Carex juncella* (Fries) Th. Fries together with the macroresidues of cotton grass, dwarf shrubs, and two *Sphagnum* species (*Sphagnum jensenii* and *Sphagnum magellanicum*) were observed at a depth of 52–54 cm. The intrusion of sedge-sphagnum peat can be evidence of thermokarst activity, which formed on a frozen mound at the turn of the new era, c. 2000 cal. a BP. Afterwards, the surficial layer of *Sphagnum fuscum* peat was formed again.

#### 5.4. Interpretation of Humification Data

The degree of peat humification is presented in Figure 4 and interpreted as an indicator for the moisture content of the local mire habitat, which also persists in the buried layers of peat. With a decrease in the moisture content of the habitat (and the moisture content of the forming peat), the degree of peat decomposition increases and the degree of humification becomes higher [32,33,50–52].

In general, the degree of humification of peat was lower in the first period of its accumulation in the Nadym peat sequence from 8000 to 5900 cal. a BP (depth of 600–300 cm), which is expressed in units of light absorption from 0.05 to 0.15 (Figure 4). Above these deposits, the degree of humification of peat is steadily increased and ranges from 0.15 to 0.45 units of light absorption. Studies in European and North American [50,52] have hypothesized

that the degree of humification of peat increases when the surface of the bog is drier and decreases when it is wetter. The nature of peat-forming plants also influences the degree of humification of peat [53]. Our study of the Nadym palsa bog sequence revealed five periods of a sharp increase in the degree of peat humification, which took place at c. 7700, 7000, 6000, 5000, 3000 cal. a BP. The sixth maximum of the degree of humification is in the present. The maxima of peat humification have different durations and amplitudes (Figure 4). The oldest maximum of the increased humification was long (about 300 years) and coincides with the deposition of a sedge–horsetail peat layer during the eutrophic stage of the mire development (Figure 4). It is likely that this maximum formed by the nature of the macrofossils. Then, at about 7000 cal. a BP, there was a second short peat humification maximum of a smaller amplitude, which was not associated with specific macrofossil composition of peat, but it sharply separates the eutrophic stage of the mire development from the subsequent mesotrophic stage. Perhaps the sharp transition from one stage of mire development to another could be caused by a short episode of freezing. The third maximum of high-amplitude peat humification was observed at c. 6100–6000 cal. a BP (depth of 320–310 cm). After it, the mire passed from the mesotrophic stage to the meso-oligotrophic string–flark mire. The fourth maximum of humification consists of a series of five short-lived maxima, the largest of which occurred at about c. 5000 cal. a BP (Figure 4), during which the degree of humification became highly variable. This series of humification maxima probably reflects the migratory nature of ridges and hollows on the bog’s surface during the oligotrophic ridge–hollow stage of development. At about 4000 cal. a BP (depth of 125 cm), the degree of humification of peat increased for the fifth time, but the steady increase in the peat humification took place approximately from c. 3000 to 2000 cal. a BP. In the same period, the rate of peat accumulation sharply decreased (Figure 3). It is possible that peat accumulation completely stopped during this period. In the upper 50 cm of the sequence, there is a sharp decrease in the degree of humification, especially at the depth of 30–10 cm. This can be related to the depth of the accretion zone in the unfrozen peat. The uppermost centimeters of peat again demonstrate an increase in the degree of peat humification on the top of the palsa bog.

##### 5.5. Quantitative Reconstruction of Paleoclimate

Quantitative paleoclimatic conditions were reconstructed in more detail from pollen data using the information–statistical method of Klimanov [47]. Reconstructions were made based only on pollen data with realistic radiocarbon dating from the depth of 650 cm and above (from 8400 cal. a BP and younger). Results of the reconstructions of mean January  $t$  ( $^{\circ}\text{C}$ ), mean July  $t$  ( $^{\circ}\text{C}$ ), and mean annual  $t$  ( $^{\circ}\text{C}$ ) are presented in Figure 9. Because of a strong decrease in the rate of peat accumulation during the past 3500 years, only a few pollen assemblages were available to reconstruct paleoclimate of that time, and quantitative reconstructions for the past 3000 yrs. have a low temporal resolution. In general, quantitative reconstructions demonstrate very small variability of mean July temperatures and remarkable variability in mean January temperatures during the past 8000 years. Mean annual temperatures were slightly higher than the present in periods 6900–6000, 4800–4000, and 1800–1300 cal. yr BP. Mean July temperatures were slightly lower than the present in periods 6900–5300 and after 2000 cal. a BP. Mean January temperatures fluctuated much more strongly, demonstrating six pronounced minima around c. 8300, 6200, 5000, 4650, 2800, and 600 cal. a BP. We assume that using only pollen data of trees in the paleoclimate reconstructions causes less variations in reconstructed July temperatures and stronger variations in reconstructed January temperatures. This is because one of the key factors limiting tree growth at the north boundary of the forest zone in West Siberia is the spreading of permafrost in soils, which is controlled by severity of winter temperatures [6,7]. Among Siberian tree species, only *Larix sibirica*, *Picea obovata*, and *Pinus sibirica* can grow in soils with permafrost [54]. *Pinus sylvestris* and *Abies sibirica* cannot. It makes pollen spectra especially sensitive to fluctuation of January temperatures and less sensitive to July temperatures. The other proxies, such as Chironomidae, can be useful for

elaboration of July temperature reconstructions in West Siberia, because the life cycle of these organisms takes place mainly during the summer season.

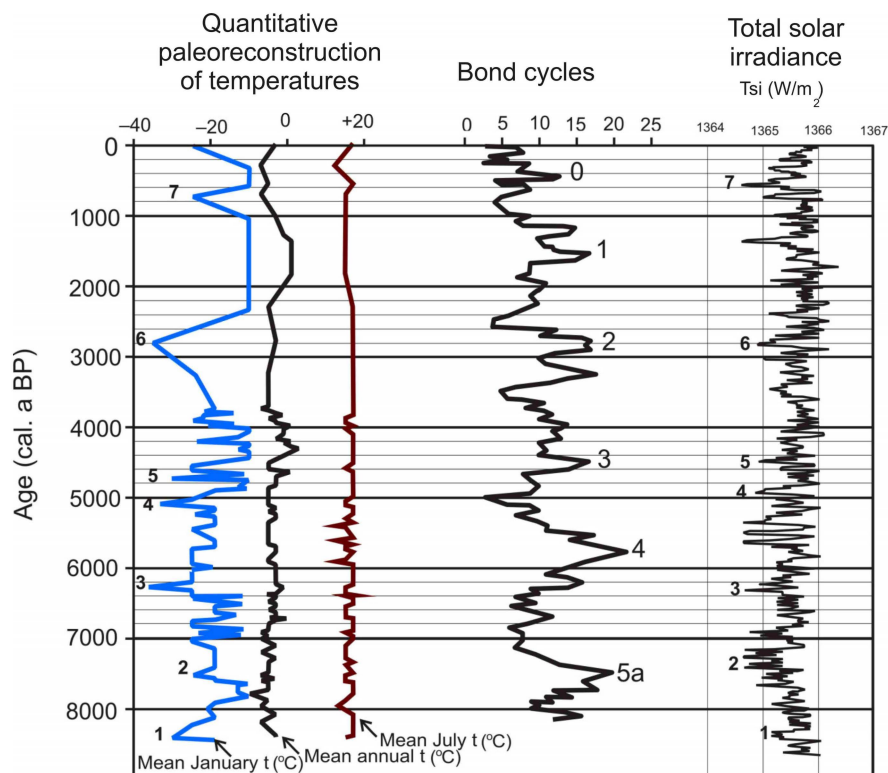


**Figure 9.** Correlation of quantitative paleoclimate reconstructions calculated with use of information–statistic method [47] based on pollen data from Nadym section with variability of global forcing: Bond cycles [55] and total solar irradiance [56].

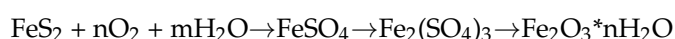
### 5.6. Holistic Synthesis of Multi-Proxy Paleoecological Data and Discussion

#### 5.6.1. Reconstruction of Lake–Mire Development of the Nadym Section in Light of Quaternary Landscape and Climate Change

In this paragraph, we follow suggestions in the conceptual framework of the strong fuzzy EHLFS (Environmental–Human–Landscape Feedback and Synergies) approach [19]. We try to take into account as many proxies as possible, using multiple lines of evidence. The lithological structure of the Nadym palsa bog sequence revealed a complex pattern of sedimentation. In addition to the influence of epicryogenic cryolithogenesis, which caused permafrost heaving, distortion of sediments through cryoturbation, our data indicate a possible interruption in sedimentation at the depth of c. 880 cm. According to sediment structure, this interruption occurs in a layer of gray-brown gyttja. As evidence of interruption, we consider (i) a series of unsuccessful radiocarbon dates obtained for sediments deeper than 800 cm (see Table 3); (ii) a pronounced cryogenic sediment microstructure at a depth below 800 cm in the form of red-brown granules (nodules) of iron–clay aggregations (Figure 2) in combination with rounded quartz granules; (iii) that the abundance of tree pollen in these deposits (Figure 4) is not consistent with other published pollen data for this area. The listed features may indicate that at the coring site, lacustrine–mire deposits of the Holocene age (the lower date of which is  $8321 \pm 45$  radiocarbon years) from the depth of about 800 cm lay on older Quaternary deposits, possibly of Kazantsevo interstadial or Karginisk–Kazantsevo time (MIS5 and MIS3). The age of these deposits turned out to be beyond the capabilities of the radiocarbon dating method. As a result, too young or modern dates from these deposits showed only the age of organic contamination that arose during drilling with a permafrost drill, which was confirmed by AMS dates obtained in

two certified radiocarbon laboratories using both bulk sediment samples and macrofossils carefully collected from sediment (see Table 3).

The second feature of the obtained 11 m long core of the studied peat–lacustrine deposits is the lack of pollen spectra of the Late Glacial and Last Glacial time. Influence of the glacial condition on sediments can be judged only indirectly from the secondary epicryogenic diagenesis of sediments deposited earlier in warmer periods. As described in Section 4.1., the deposits in the Nadym sequence below 900 cm have a red-brown color and a granular texture. The analysis revealed that iron is the main chemical element in them. A granulate texture and prevailing of iron in the chemical composition of these granules resemble secondary epicryogenic diagenesis of sediments described in Yakutia at the cold pole of Siberia [57,58]. Such transformations in sediment saturated with iron oxides in the form of iron–clay aggregates (grains or nodules) occur in neutral and alkaline environments under subaerial conditions of a sharply continental climate. According to studies [57,58], the cryogenic aggregate is an association of clay and fine sand particles bound by iron hydroxides, which does not disaggregate in water. Colloidal limonite, which is formed in the process of cryogenic destruction of iron-containing minerals, such as biotite, chlorite, siderite, pyrite, etc., serves as a kind of glue that fastens particles into aggregates.



A cryogenic aggregate is formed through the layering of clay particles and iron hydroxides on microparticles of the sandy fraction of quartz or feldspar [58]. Thus, the granules that we observe in the lower red-brown deposits of the Nadym sequence (Figure 2a–c) seem to represent this type of cryogenic formations. Oxidation processes can occur only in the presence of oxygen [58], which means that these ancient deposits were under subaerial conditions and severe sharp continental climate for a long time before lake peat sedimentation in the Holocene. Presently, the study area is characterized by moderate continental climate.

The following question arises: what could have caused the absence of Stadial-age sediments in the Nadym section under study? We argue that this can be caused by the cryoarid conditions that existed in the glacial time in the north of western Siberia [59]. Mineral particles in the lower parts of the Nadym sequence are rounded (Figure 2a–c), likely caused by aeolian action during glacial conditions [59]. This process was probably accompanied by a neotectonic uplift of the Nadym area, because the territory of Nadym during the Kargink cryochron was in an area of marginal compensatory deflection caused by the weight of a glacier located to the northwest [60–63]. The level of the Kara Sea in MIS3–MIS2 decreased by 110–120 m [62–64] and large areas of the shelf were drained. Under the weight of the glacier, the earth’s crust sagged, causing the adjacent territories to bulge. As a result, the currently low-lying area was uplifted and eroded. With the disappearance of the glacier in the Late Glacial period, areas remote from the centers of glaciation (the southern part of Yamal and Gydan peninsular land) experienced a sea level rise to a few meters above the present level, followed by a slow fall [63]. It is possible that the territory of Nadym (adjacent to Yamal and Gydan) in the Late Glacial period experienced similar subsidence, leading to a marine incursion, after which the sea receded. Evidence of the marine interval in the evolution of sedimentary deposits of the Nadym sequence can be numerous remains of brackish-water diatoms, radiolarians, and silicoflagellates at the depth of 650–850 cm (8500–9800 cal. a BP) (Figure 7). Another option that could explain the abundance of these remains in combination with the findings of exotic Neogene pollen (Figure 6) may be the redeposition of these remains from Neogene and even Paleogene deposits, found in the north of western Siberia [38,42]. The landscapes of West Siberia during the Late Glacial–Early Holocene period were likely half-bared as a result of the Last Glacial Maximum and susceptible to erosion. Together with progressively increasing atmospheric precipitation and subsidence of the landscape, the erosion of the Neogene sediments may have led to the redeposition of ancient pollen and NPPs in the depression of the lake basin. Diatom valves are highly fragmented, but redeposited exotic Neogene pollen is very well preserved (Figures 6 and 7). The redeposition of ancient pollen and

diatoms must have stopped when lake sedimentation changed to peat accumulation. This hypothesis, however, must be tested through additional research in the Nadym area. The same concerns the alternative (less likely) hypothesis about a warm and moist Late Glacial and Early Holocene period with lush coniferous forests spread in the subarctic Nadym area.

The second stage in development of landscape represented by pollen assemblages of LPZ-2 is similar to LPZ-1 through plant composition, but with narrower ecological tolerances. In this stage, the xerophytic species of *Artemisia* and Chenopodiaceae and pollen shrub birch (*Betula nana*) together with aquatic and wetland plants—*Typha* and *Myriophyllum*—play a greater role. The radiocarbon dating of LPZ-2 is not problematic, covering 9800–8400 cal. a BP of the Early Holocene. It is during this period that the pollen spectra are enriched by diatoms, exotic pollen, and NPP signaling erosional inputs from surface run-off into the lake basin, including charcoal, *Glomus*, and fungal spores. We assume that during the Early Holocene, the north part of West Siberia was rather bare after the last Stadial and experienced increasing humidification of climate, causing redeposition of exotic pollen by surface water run-off. Exotic pollen includes both very old pollen from Neogene and pollen redeposited from Middle Quaternary interglacial periods. Thus, possibly, the pollen spectra of LPZ-2 became enriched by pollen of *Picea* and *Pinus*. Possibly, only pollen of Poaceae, Chenopodiaceae, *Betula nana*, and *Lycopodium* spores originates from vegetation of the Early Holocene. It is possible that pollen spectra from this part of the sequence are mostly redeposited, and should only be used for reconstruction of vegetation in the Early Holocene with great caution. Similarity between pollen spectra of LPZ-2 and LPZ-1 (see PCA biplot in Figure 8) supports this hypothesis about a mixed origin.

The third stage in the landscape development (LPZ-3) has a large proportion of pollen of *Betula pendula* and *Carex*. During this stage, 8200–6000 cal. a BP, the landscapes of Nadym began to be dominated by birch swamp forests, combined with sedge thawed bogs in eutrophic and mesotrophic stages. On the margins of the swamps, thickets of alder (*Alnaster*), whitehead (*Filipendula*), and burnet (*Sanguisorba*) were common. In the swamps themselves, there were lawns of sedge (*Carex lasiocarpa*) alternated with clusters of *Menyanthes* and *Comarum palustre* reflecting specific ‘noda’ (type of mire vegetation according to [65]). We argue that these pollen assemblages have an autogenic origin and represent the real vegetation existing during the middle Holocene in the study area. The common pollen taxa reflect spreading of birch forests and complex meso-oligotrophic mires, first string–flark and later ridge–hollow patterned mires. In the hollows, trefoil (*Menyanthes trifoliata*) and scheuchzeria (*Scheuchzeria palustris*) grew, and on the ridges, cloudberry (*Rubus chamaemorus*) grew.

The fourth stage in the development of landscape is reflected in LPZ-4. An area of pollen assemblages of LPZ-4 is located in the bottom part of the PCA biplot. The leading pollen components in it are *Pinus sylvestris* and Ericaceae. It reflects dominance of pine forests and oligotrophic frozen peatland—the palsa bog at the study site and, possibly, other areas of Nadym. In these assemblages, pollen of *Pinus sylvestris*, Ericaceae, *Drosera*, *Pinus sibirica*, and *Larix sibirica* is connected by positive correlation with each other, also reflecting a specific ‘noda’ of the palsa bog. It is worthwhile to note that *Pinus sibirica* and *Larix sibirica* can grow in soils and peats with permafrost. Therefore, an increase in their participation in the forest may reflect the spread of permafrost.

#### 5.6.2. Joint Reconstruction of Landscape, Climate, Mire Development, and Vegetation Change during the Holocene Based on Paleoecological Data and Quantitative Reconstructions of Paleoclimate

Because of a lack of reliable dating for the bottom sediments in the studied sediment core, we only made reconstructions of paleolandscape from c. 9400 cal. a BP to the present. Thus, this paragraph outlines the detailed development of the landscape pattern after the last deglaciation. Numerous lakes existed in the study area in the Early Holocene. Increased precipitation combined with readily erodible surfaces after the Last Glacial period led to deposition of older material in the lake basin. It is possible that some part of coniferous pollen (spruce, Scots pine, and Siberian pine) in sediments deeper than 700 cm is, in part,

redeposited from older Quaternary sediments. Unfortunately, we cannot separate Holocene and redeposited older conifer pollen visually. All conifer pollen accumulated at this stage of development has very good preservation. In addition, these deposits contain numerous findings of *Larix* and *Picea* stomata that are evidence of local forest stands near a lake. On the other hand, stomata can be redeposited together with all exotic pollen. In this regard, we tend to consider the spore–pollen spectra from deposits deeper than 700 cm as mixed and not reflecting the real local vegetation cover of the Early Holocene. However, landscapes forested by spruce and birch (*Betula* sect. *Albae*) have been reconstructed using pollen data from a site in the Pur–Taz interfluvium near the arctic circle [66] for the period c. 9800 cal. a BP. In any case, because it is impossible to separate redeposited conifer pollen from Holocene conifer pollen, we do not use pollen spectra of sediments older than 8300 cal. a BP for quantitative paleoclimate reconstruction.

At about 8300 cal. a BP (depth of 650 cm), there were significant changes in the landscape. The lake, infilled with sediments, turned into a swamp and peat accumulation initiated. By this time, redeposited pollen of exotic pollen and diatom valves disappeared from the samples. We believe that only spore–pollen spectra from peat deposits adequately reflect changes in the vegetation. Based on these pollen data, we performed quantitative paleoclimate reconstructions using the Klimanov information–statistical method [47], results of which are presented in Figure 9a. During this time in the dynamics of the vegetation cover of the study area, there were two main phases, reflected in LPZ-3 and LPZ-4 with their sub-phases (Figure 5):

1. Phase of spruce–birch forests with open meadow spaces (LPZ-3a). At around c. 8400–7700 cal. a BP, open herbaceous meadows probably still played a significant role (based on the abundance of grass pollen). During this period, the overgrowing lake infilled and turned into a eutrophic wet swamp, in which common mosses and species of cotton grass (*Eryophorum*) and horsetail (*Equisetum*) dominated (Figure 4). At the beginning of peat accumulation, the low degree of humification indicates waterlogged mire conditions. A layer of peat with sharply increased humification seems to connect with remains of herbal plants (*Carex cespitosa*, horsetail, *Menyanthes*) [50,53]. These species assemblages reflect unstable hydrological environments, which form heterogeneous microtopography in the form of tussocks of sedges, which are raised above the water level, with bogbean and horsetail in wet areas between them. Such conditions eventually cause increased decomposition of plant remains and increased humification of forming peat. Quantitative reconstruction of paleoclimate using the Klimanov information–statistical method showed that mean annual temperatures were close to modern ones, but mean January temperatures were lower than modern ones at the beginning of this phase (8400–8200 cal. a BP) and higher than modern ones at the end of this phase (Figure 9). Thus, data from the Nadym core are in agreement with an episode of global cooling of 8200 cal. a BP, reconstructed in a number of studies on temperature change in the northern hemisphere [67].
2. The phase of maximum spread of spruce forests (LPZ-3b). This phase lasted from c. 7700 to 6500 cal. a BP. Based on available proxy data, this was the Holocene optimum, during which winter temperatures were higher compared to modern ones (Figure 9). This probably contributed to the decrease in or complete disappearance of permafrost in soils, which, in turn, favored the northward shifting of taiga forests. Reconstructions of winter temperatures using the Nadym sequence are generally higher than modern ones, and were highly variable. During this period, the mire was in the eutrophic stage of development and eutrophic hydrophilic species of sphagnum *Sphagnum teres* spread, forming wide wet lawns. It is worthwhile to note that *Sphagnum teres* expansion coincides with the second peak of the increase in the degree of humification of peat, dated c. 7500 cal. a BP. This was followed by a sharp change from *Sphagnum teres* to the less hydrophilic mesotrophic *Sphagnum angustifolium* after the third maximum of humification (Figure 4). The last maximum in humification coincides with the series of decreases in total solar irradiance [56] (Figure 9c).

3. The phase of coniferous–birch forests (LPZ-3c) lasted from 6500 to 4500 cal. a BP. During this 2000-year period, birch dominated the forest cover, and the role of spruce was significantly reduced compared to the previous period. At the same time, the role of the Siberian pine in the forests began to increase. This was a long and climatically stable period in which average global temperatures of the northern hemisphere gradually decreased [67,68]. Our quantitative temperature reconstructions using the information–statistical method of V.A. Klimanov (Figure 9) indicate mean annual temperatures that are stable and similar to modern ones. January temperatures decreased compared with the previous phase and were also similar to modern ones. Against this background of relatively stable temperatures, there were three episodes of a strong decrease in January temperatures (colder than modern), c. 6200, 5000, and 4650 cal. a BP. These episodes of low winter temperatures had a decisive influence on the endogenic development of the mire. The first episode of cooling, c. 6200 cal. a BP, is close to the fourth maximum in peat humification (Figure 4). Although this short-term cooling of the climate did not cause any noticeable changes in the vegetation cover of dry areas, it stimulated the transition of the mire from the mesotrophic stage to the stage of the oligotrophic ridge–hollow bog. The second episode of a sharp decrease in winter temperatures, which took place at c. 5000 cal. a BP, was also accompanied by a series of maxima in the degree of peat humification. As mentioned above, we believe that the alternation of peat layers composed of the remains of hydrophilic sphagnum mosses (*Sphagnum jensenii*, *Sph. Angustifolium*, and *Sph. balticum*) with layers of cotton grass and shrub peat during this period reflects the formation of a ridge–hollow micro relief on the bog. Frost heaving of peat could repeatedly occur in the ridges. They are marked by peaks of peat humification. The frequency of frost heaving increased toward the end of phase LPZ-3c, when there was a noticeable decrease in the average global temperature of the northern hemisphere [68]. A strong cryoturbation of these peat layers at the depth of 125–210 cm (3000–4800 cal. a BP) and deeper than 260 cm (over 5500 cal. a BP) is evidence of repeated epigenetic freezing of heavily waterlogged peat layers (Figure 4).
4. The birch–pine forest phase (LPZ-4) covers the last 4500 cal. a BP. During this period, the abundance of Siberian pine and Scots pine increased sharply in the vegetation cover of the study area, while spruce and birch decreased. As noted above, since that time, the rate of peat accumulation has sharply slowed down. A sharp change in the macrofossil composition of peat from the remains of hydrophilic plants to more xerophytic plants of oligotrophic ecology took place at the depth of 160 cm at about 4400 cal. a BP and probably marks the freezing of the mire and the beginning of the formation of the palsa bog (Figure 3). Probably due to freezing and bulging of the peat bog, its surface dried up to such an extent that the main types of peat formers (bog mosses and common mosses) perished. The lichens that were established in their place did not form peat, but contributed to the decomposition of the previously deposited peat. The degree of peat humification increased sharply at a depth of 80 cm (about 3000 cal. a BP) (Figure 4). Siberian pine settled on its bulk surface. Individual Siberian pine trees with full crowns are presently found on the palsa bogs of the northern taiga (Supplemental Materials, Figure S1). A particularly strong decrease in winter temperatures according to the reconstructions of the Nadym sequence took place at c. 3000 cal. a BP (Figure 9). In the period of 3000–2000 cal. a BP, almost no peat was formed on the studied bog, and it is this thin layer of peat that has the maximum degree of humification over the entire period of peat accumulation. Samples from this depth (60–70 cm) have high concentrations of fine mineral detritus and had a relatively high content of microcharcoal particles. These features indicate long-term exposure of the surface of the peat bog without peat accumulation. Above and below this layer, mineral and charcoal pollution disappears. Perhaps this is a reflection of the increasing continentality of the climate, which would feature both colder winters and hotter summers. This does not contradict our reconstruction of the average January

and average July temperatures for this time (Figure 9). The latter could stimulate thermokarst subsidence on the surface of the palsa bog. Evidence of such thermokarst activity is a layer of peat formed by the remains of sedge and cotton grass at the depth of 62–52 cm. Afterwards, the accumulation of *Sphagnum* peat from the remains of *Sphagnum fuscum* resumed. But the peat of the upper 50 cm has a low degree of humification, which increases only in the uppermost samples. These layers probably reflect the features of the accretion zone, complicated by a new frost-heave of the bog surface during the cooling period of the Little Ice Age (LIA).

In general, quantitative reconstructions of the paleoclimate using the information–statistical method of V.A. Klimanov showed that episodes of a strong decrease in January temperatures occurred at c. 8200, 6200, 5000, 4650, and 2800 cal. a BP and coincide with the general trend of decreasing global temperatures in the northern hemisphere, which began after 6000 cal. a BP [66] and with main Holocene cold events at 8200, 6300, 4700, and 2700 cal. a BP [68]. It is possible that before 3000 cal. a BP, frost heaving led to the formation of elevated strings and later ridges. But this permafrost did not exist for long, and the mire as a whole remained thawed, as indicated by the macrofossil composition of peat, which is formed mostly of remains of hydrophilic mire plants (Figure 4). Only with the beginning of the third millennium BP, the cooling turned out to be so strong and prolonged that the mire system passed into a new state: the palsa bog. The transition from a thawed mire system to a palsa bog was caused by a strong decrease in winter temperatures at c. 2800 cal. a BP, which occurred during the period of low solar activity (TSI minimum number 6). At the same time, the epigenetic freezing of the waterlogged peat layers caused strong cryoturbation, which we observed on the cleared exposure of the peat bog (Figure 4, Table 3). Reconstruction of average July temperatures indicates an increase during the Medieval period and a sharp decrease during the Little Ice Age (Figure 9) at about 500 cal. a BP. But the last assumption needs to be confirmed through additional studies, because in the Nadym section, pollen data for the past 3000 years are represented only by a few samples. More high-resolution paleoecological data are needed for this time interval.

It should be noted that the amplitude of the reconstructed mean January temperatures is too large (almost 25 °C). Perhaps this is caused by a too large set of training-set samples used in Klimanov's information–statistical reconstruction model [47]. Around 800 samples from 200 points throughout the entire flat territory of the former USSR were used. This area is very diverse in terms of climatic characteristics and the role of individual plant species in the vegetation cover. We believe that with a narrower region for the training set of samples, for example, including only western Siberia, more accurate quantitative reconstructions of the paleoclimate can be made. It is probable that the reconstructed paleoclimate correctly reflects the trends that have taken place, since it is consistent with the general trend of the global average annual temperatures of the northern hemisphere [67]. Most of the reconstructed events of a sharp decrease in January temperatures based on Nadym pollen data are in good agreement with known global cold events [68].

Comparison of pollen-based quantitative reconstructions of paleoclimate for the Nadym site with Bond cycles [55,68] indicates that the last, most significant of the reconstructed cooling events at 2800 cal. a BP, which led to the transition of the mire to a frozen state of the palsa bog, coincided with Bond cycle number 2. Bond cycle numbers 3, 4, and 5a coincided with the formation of an oligotrophic ridge–hollow complex in the mire and caused first episodes of frost heaving in ridges. It is also possible to correlate the reconstructed decrease in January temperatures at 8200 cal. a BP with Bond cycle number 5b.

Comparison of quantitative climate reconstructions based on the Nadym sequence with the total solar irradiance (TSI) [56] demonstrates that the identified episodes of a sharp drop in January temperatures coincide with solar activity minima (Figure 9). These matches are marked with numbers from 1 to 7 in January temperature (°C) reconstructions (Figure 9a) and in solar activity (Figure 9c). In the sixth millennium BP, two sharp minima of solar activity coincide with a decrease in mean July temperatures in the paleoclimate

reconstruction. The cooling at 2800 cal. a BP (marked by 6) is clearly expressed both in data of solar irradiance and in reconstruction of January temperatures. Also, in the Nadym sequence, the decrease in annual January temperatures marked with the number 7 coincides with the Wolf minimum in solar activity.

Thus, we can conclude that most cases of a sharp drop in mean January temperatures in the Nadym region coincide with a decrease in solar activity and with periodicity of Bond cycles. The conducted studies show how these factors of global climate change influenced the subarctic environment of western Siberia at the regional (change in vegetation cover) and local (swamp successions and freezing of peat bogs) levels. The paleoecological data from the Nadym peat sequence are in agreement with the “phase theory” of Barber [49,65]. According to this theory, climate controls the growth of raised bogs. Phase shifts in peat macrofossil composition (*Sphagnum* “succession”, or sudden changes between major assemblage types) are the result of climate shifts. We can see these sudden changes in the macrofossil composition of the Nadym peat sequence, but they are superimposed on autogenic successional development of the mire. It is probable that during cooling periods, the strengthening Siberian anticyclone pushed back the warmer moisture-bearing western currents, bringing colder weather with little moisture (snow). The decrease in winter precipitation contributed to deeper and longer freezing of soils and peatlands, which did not have time to thaw in the summer [7]. In such periods, the larger areas of upland and mires began to be affected by frost heave, despite the fact that the temperature of the summer seasons remained fairly stable—approximately equal to the present. It is also possible that Klimanov’s paleoclimate reconstruction method is less sensitive to changes in summer temperatures than to changes in winter temperatures due to the ecology of tree species. Another biological proxy such as chironomid head capsules would be helpful in reconstruction of summer temperatures in West Siberia during the Holocene.

## 6. Conclusions

The multi-proxy high-resolution paleoecological studies of the sediments of the palsa bog Nadym located in the north of western Siberia on the border of the northern taiga and forest–tundra zones revealed a complex picture of changes in the landscape and vegetation cover of this region over the Late Quaternary period. The following paleogeographic milestones in the development of the landscape, climate, and vegetation of the study area were noted:

1. Deposits of the palsa bog have a thickness of 1050 cm, including 610 cm of peat, and are underlain by 440 cm of lacustrine and mineral deposits. Radiocarbon-dated Holocene deposits cover the upper 790 cm of sediments (including peat and lake sediments accumulated during the past 9400 cal. years). The radiocarbon dating of underlying sediments (from 790 to 1050 cm) failed, demonstrating a too young or modern age. To explain this phenomenon, we assume that these sediments can be too old for the radiocarbon method containing radiocarbon ‘dead’ material. This hypothesis can be supported by 10 unsuccessful AMS radiocarbon dates and through composition of pollen and NPP spectra from these sediments. An alternative hypothesis suggests very warm and humid climate in the Late Glacial and Early Holocene period in the north of West Siberia favorable for spreading extensive coniferous forests. Further studies of additional sediment cores have to be conducted in this area to confirm one of the hypotheses.
2. Well-dated Holocene lacustrine deposits underlying the peat in the Nadym sequence are enriched in redeposited pollen of the Neogene and Paleogene age, as well as remains of brackish and freshwater diatoms. We interpret this as evidence of an increasingly wet climate in combination with glacio-isostatic subsidence of the landscape, leading to lake formation during the Early Holocene. This caused run-off and erosion from areas of higher relief and redeposition of exotic pollen and diatom shells in a lake.

3. The pollen data of the Nadym section are arranged in four local pollen zones (LPZs). The two bottom pollen zones LPZ-1 and LPZ-2 were distorted by redeposited pollen. Zones LPZ-3 and LPZ-4 reflect vegetation history more correctly. Based on pollen and macrofossil data, the history of dry land and mire vegetation was reconstructed.
4. Because of the complex history of sediments underlying the peat deposits, a quantitative reconstruction of paleoclimate was applied only to pollen data covering well-dated peat and lacustrine deposits above 790 cm (after c. 8200 cal. a BP). The reconstruction indicated seven periods of a strong decrease in the mean January temperatures and the relative stability of the mean July temperatures over this period.
5. Most of the episodes with a sharp drop in mean January temperature reconstructed from the pollen data of the Nadym sequence coincide with periods of reduced solar activity [56] and they coincide with Bond cycles. Our results suggest a leading role for changes in solar radiation in the decrease in winter temperatures and in the formation of permafrost in soils and mires in the study area. Our reconstruction of the Nadym mire development confirms the “phase theory” of Barber [49,65], according to which climatic changes drive the growth of a raised bog. Impact of climate, however, is superimposed on autogenic successional development of the mire.

**Supplementary Materials:** The following supporting information can be downloaded at: <https://www.mdpi.com/article/10.3390/quat7010001/s1>, Figure S1: Landscapes of Nadym area and coring site; Figure S2: Landscapes of Nadym area; Table S1: Exact depths for each sample.

**Author Contributions:** Conceptualization of research was made by T.B. and O.P.; research methodology was chosen by T.B.; software applied by N.S.; validation was made by T.B., N.S. and O.P.; formal analysis performed by T.B., N.S. and H.-C.L.; pollen and macrofossil investigation performed T.B. and N.S.; resources for field work and laboratory work provided T.B. and O.P.; for data curation were responsible T.B. and N.S.; writing—original draft preparation was made by T.B.; in writing—review and editing took part O.P.; graphics, diagrams and figures were made by T.B. and N.S.; supervision and project administration performed T. B.; funding acquisition belongs to T.B. and O.P. All authors have read and agreed to the published version of the manuscript.

**Funding:** This work was funded by Russian Scientific Foundation grand № 23-27-00217.

**Data Availability Statement:** All data generated during this study are included in this published article and its Supplementary Information Files.

**Acknowledgments:** Authors are grateful to Gravis A.G. and Berdnikov M.N. for help in the field and to M.G. Magur for performing the macrofossil analysis of peat, and to Leon Clarke for help with AMS dating of a few samples. Special thanks we give to our colleague Maarten van Hardenbroek from Newcastle University (UK) for his kind agree to correct English of manuscript. The authors are also grateful to four anonymous reviewers for their careful reading of the manuscript and for their valuable comments and advice, which allowed us to improve the work.

**Conflicts of Interest:** The authors declare no conflict of interest.

## References

1. Groisman, P.V.; Blyakhrachuk, T.A.; Chernokulsky, A.V. Climate Change in Siberia. In *Regional Environmental Changes in Siberia and their Global Consequences*; Groisman, P.V., Gutman, G., Eds.; Springer Environmental Science and Engineering: Dordrecht, Germany, 2013; pp. 57–107.
2. Callaghan, T.V.; Shauyko, O.; Kirpotin, S.N. Siberian environmental change: Synthesis or recent studies and opportunities for networking. *Ambio* **2021**, *50*, 2114–2127. [[CrossRef](#)] [[PubMed](#)]
3. Stocker, T.F.; Qin, D.; Plattner, G.-K.; Tignor, M.; Allen, S.K.; Boschung, J.; Nauels, A.; Xia, Y.; Bex, V.; Midgley, P.M. (Eds.) IPCC, Summary for Policymakers. In *Climate Change 2013: The Physical Science Basis. Contribution of Working Group I to the Fifth Assessment Report of the Intergovernmental Panel on Climate Change*; Cambridge University Press: Cambridge, UK; New York, NY, USA, 2013.
4. Khrustalev, L.N.; Klimenko, V.V.; Emel’yanova, L.V.; Ershov, E.D.; Parmuzin, S.Y.; Mikushina, O.V.; Tereshin, A.G. Dynamics of permafrost temperature in southern regions of cryolithozone under different scenarios of climate change. *Kriosf. Zemli* **2008**, *12*, 3–11.
5. Slater, D.M.; Lawrence, D.M. Diagnosing present and future permafrost from climate models. *J. Clim.* **2013**, *26*, 5608–5623. [[CrossRef](#)]

6. Kirpotin, S.N.; Blyakharchuk, T.A.; Vorobiev, S.N. The dynamics of the Subarctic flat-hillock bogs of the West Siberian Plain as an indicator of global climatic changes. *Tomsk. Univ. Bull. Ser. Biol. Sci.* **2003**, *7*, 122–134.
7. Ponomereva, O.E.; Gravis, A.G.; Berdnikov, N.M.; Blyakharchuk, T.A. Climate change, frost action, and permafrost-related processes in the northern taiga region of West Siberia. In Proceedings of the Tenth International Conference on Permafrost, Salekhard, Russia, 25–29 June 2012; Volume 2, pp. 343–347.
8. Bickaborn, B.K.; Smith, S.L.; Noetzli, J.; Matthes, H.; Vieira, G.; Streletskiy, D.A.; Schoeneich, P.; Romanovsky, V.E.; Lewkowicz, A.G.; Abramov, A.; et al. Permafrost is warming at a global scale. *Nat. Commun.* **2019**, *10*, 264–278. [[CrossRef](#)] [[PubMed](#)]
9. Romanovsky, V.; Smith, S. Permafrost thermal state in the polar Northern hemisphere during the international polar year 2007–2009: A synthesis. *Permafrost Periglacial Process* **2010**, *21*, 106–116. [[CrossRef](#)]
10. Streletskiy, D.; Anisimov, O.; Vasiliev, A. Permafrost degradation. In *Snow and Ice-Related Hazards and Disasters*; Haeberli, W., Whiteman, C., Shroder, J.F., Eds.; Elsevier Inc.: Amsterdam, The Netherlands, 2015; pp. 303–344. [[CrossRef](#)]
11. Ponomareva, O.E.; Moskalenko, N.G.; Berdnikov, N.M.; Blyakharchuk, T.A.; Bochkarev, Y.N.; Ustinova, E.V.; Gravis, A.G.; Lobotrosova, S.A.; Matyshak, G.V.; Popov, K.A.; et al. Transformation of cryogenic geosystems in the southern part of the Arctic in Western Siberia under the influence of climate warming. *Sci. Bull. Yamal-Nenets Auton. Okrug* **2015**, *2*, 123–130.
12. Turnocai, C.; Candell, J.; Achuur, E.; Kuhry, P.; Mazhitova, G.; Zimov, S. Soil organic carbon pools in the northern circumpolar permafrost region. *Glob. Biogeochem Cycles* **2009**, *23*, GB2023. [[CrossRef](#)]
13. Wisser, D.; Marchenko, S.; Talbot, J.; Treat, C.; Frohling, S. Soil temperature response to 21-st century global warming: The role of and some implications for peat carbon thawing permafrost soils in North America. *Earth Syst. Dyn.* **2011**, *2*, 161–210. [[CrossRef](#)]
14. Christensen, T.R.; Arora, V.K.; Gauss, M.; Höglund-Isaksson, L.; Parmentier, F.-J.W. Tracing the climate signal: Mitigation of anthropogenic methane emissions can outweigh a large Arctic natural emission increase. *Nat.-Sci. Rep.* **2019**, *9*, 1146–1153. [[CrossRef](#)]
15. Routh, J.; Hugelius, G.; Kuhry, P.; Filley, T.; Tillman, P.K.; Becher, M.; Crill, P. Multi-proxy data of soil organic matter dynamics in permafrost peat deposits revealed vulnerability to climate change in the European Russian Arctic. *Chem. Geol.* **2014**, *368*, 104–117. [[CrossRef](#)]
16. Mel'nikov, V.P. *Complex Monitoring of Northern Taiga Geosystems in Western Siberia*; Academic publishing house "Geo": Novosibirsk, Russia, 2012.
17. Gallego-Sala, A.V.; Charman, D.J.; Brewer, S.; Page, S.E.; Prentice, I.C.; Friedlingstein, P.; Moreton, S.; Amersbury, M.J.; Beilman, D.W.; Björck, S.; et al. Latitudinal limits to the predicted increase of the peatland carbon sink with warming. *Nat. Clim. Chang.* **2018**, *8*, 907–913. [[CrossRef](#)]
18. Walter Anthony, K.M.; Zimov, S.A.; Grosse, G.; Jones, M.C.; Anthony, P.M.; Chapin, F.S., III; Finlay, J.C.; Mack, M.C.; Davydov, S.; Frenzel, P.; et al. A shift of thermokarst lakes from carbon sources to sinks during the Holocene epoch. *Nature* **2014**, *511*, 452–456. [[CrossRef](#)] [[PubMed](#)]
19. Rull, V. Strong Fuzzy EHLFS: A general Conceptual Framework to Address past Records of Environmental, Ecological and Cultural Change. *Quaternary* **2018**, *1*, 10. [[CrossRef](#)]
20. Ershov, E.D. *Geokriologiya SSSR. Zapadnaya Siber' (Geocryology of the USSR. Western Siberia)*; Nedra: Moscow, Russia, 1989.
21. Mel'nikov, E.C. *Landscapes of the Permafrost Zone of the West Siberian Gas-Bearing Province*; Nauka: Novosibirsk, Russia, 1983.
22. Streletskaya, I.D.; Pismeniuk, A.A.; Vasiliev, A.A.; Gusev, E.A.; Oblogov, G.E.; Zadorozhnaya, N.A. Formation of ice rich permafrost and underground ice in the Late Neopleystic-Holocene in the north of Western Siberia. In *Routes of Evolutionary Geography. Proceedings of the 2nd Scientific Conference in Memory of Prof. A.A. Velichko (Moscow, November 22-25, 20210 V.2)*; Institute of Geography RAS Press: Moscow, Russia, 2021; pp. 377–380.
23. Moskalenko, N.G.; Ponomareva, O.E. Changes in vegetation and geocryological conditions of heaving mounds disturbed by linear construction in the northern taiga of Western Siberia. *Earth's Cryosphere* **2004**, *8*, 10–16.
24. Blaauw, M. Methods and code for 'classical' age-modelling of radiocarbon sequences. *Quat. Geol.* **2010**, *5*, 512–518. [[CrossRef](#)]
25. Christen, J.A.; Perez, E.S. A new robust statistical model for radiocarbon data. *Radiocarbon* **2009**, *51*, 1047–1059. [[CrossRef](#)]
26. Kulikova, G.G. *A Short Guide to Botanical Analysis of Peat*; Nedra: Moscow, Russia, 1974.
27. Dombrovskaya, A.V.; Koreneva, M.M.; Tyuremnov, S.N. *Atlas of Plant Macrofossils Found in Peat*; Gosenergoizdat Press: Moscow-Leningrad, Russia, 1959.
28. Savich-Lyubitskaya, L.L.; Smirnova, Z.N. *Key to Sphagnum Mosses of the USSR*; "Nauka" Press: Leningrad, Russia, 1968.
29. Kats, N.Y.; Kats, S.V.; Skobeeva, E.I. *Atlas of Plant's Remnants in Peat*; Nedra Publ.: Moscow, Russia, 1977.
30. Mul'diyarov, E.Y. *Key to Leaf-Stem Mosses of the Tomsk Region*; Tomsk University Press: Tomsk, Russia, 1990.
31. Revushkin, A.S. *Reference Book of Plants of the Tomsk Region*; Publishing house of Tomsk University: Tomsk, Russia, 2014.
32. Chambers, F.M.; Beilman, Z.Y. Methods for determining peat humification and for quantifying peat bulk density, organic matter and carbon content for palaeostudies of climate and peatland carbon dynamics. *Mires Peat* **2011**, *7*, 1–10.
33. Caseldine, C.J.; Baker, A.; Charman, D.J.; Hendeon, D.A. comparative study of optical properties of NaOH peat extracts: Implication for humification studies. *Holocene* **2000**, *10*, 649–658. [[CrossRef](#)]
34. Grichuk, V.P.; Zaklinskaya, E.D. *Analysis of Fossil Pollen and Spores and its Application in Paleogeography*; Geografizdat Press: Moscow, Russia, 1948.
35. Kupriyanova, L.A.; Aleshina, L.A. *Pollen of Dicot Plant of the Flora of the European Part of the USSR*; Nauka Press: Leningrad, Russia, 1978.

36. Bobrov, A.E.; Kupriyanova, L.A.; Litvintseva, I.D.; Tarasevich, V.F. *Spores of Fern-Like and Monocotyledonous Flora of the European Part of the USSR*; Nauka Press: Leningrad, Russia, 1983.
37. Moore, P.D.; Web, J.A.; Collinson, M.E. *Pollen Analysis*; Blackwell Science Ltd.: London, UK, 1991.
38. Volkova, V.S.; Panova, L.A. Palynological characteristics of the Neogene deposits of Western Siberia. In *Cenozoic Palynology*; Volkova, V.S., Ed.; Nauka Press: Novosibirsk, Russia, 1975; pp. 34–52.
39. Boitsova, E.P.; Panova, L.A.; Бойцова, Е.П.; Панова, Л.А. On the issue of the boundary between the Cretaceous and Paleogene systems in the south of Western Siberia. In *Cenozoic Palynology*; Volkova, V.S., Ed.; Nauka Press: Novosibirsk, Russia, 1976; pp. 89–93.
40. Ananova, E.N. *Pollen in the Neogene Deposits of the South of the Russian Plain*; Leningrad University Press: Leningrad, Russia, 1974.
41. Kul'kova, I.A.; Laukhin, S.A. Palynology of the Paleogene deposits of the Yenisei Ridge. In *Cenozoic Palynology*; Volkova, V.S., Ed.; Nauka Publishing House: Novosibirsk, Russia, 1975; pp. 98–99.
42. Paramonova, N.V. Materials by diatom algae from Palaeogene deposits of the north of West Siberia. In *Paleophytological Sbornik*; Samoilovich, S.R., Ed.; Nedra Press: Moscow, Russia, 1965; pp. 234–246.
43. Kramer, K.; Lange-Bertalot, H. *Bacillariophyceae 3 Teil. Centrales, Fragillariaceae, Eunotiaceae*; Spektrum Akademischer Verlag: Berlin/Heidelberg, Germany, 1991.
44. Van Geel, B. A palaeoecological study of Holocene peat bog sections in Germany and The Netherlands. *Rev. Palaeobot. Palynol.* **1987**, *25*, 1–120. [[CrossRef](#)]
45. Van Geel, B.; Bohncke, S.J.P.; Dee, H. A palaeoecological study of an upper Late Glacial and Holocene sequence from “De Borchert”, The Netherlands. *Rev. Palaeobot. Palynol.* **1981**, *31*, 367–448. [[CrossRef](#)]
46. Sweeney, C.A. A key for identification of stomata of the native conifers of Scandinavia. *Rev. Palaeobot. Palynol.* **2004**, *128*, 281–290. [[CrossRef](#)]
47. Klimanov, V.A. Connection of subfossil spore-pollen spectra with modern climatic condition. *Izv. Akad. Nauk. SSSR. Ser. Geogr.* **1981**, *5*, 101–114.
48. Grimm, E.C. *TGView Version 2.0.41*; Illinois State Museum Research and Collections Center: Springfield, IL, USA, 2004.
49. Barber, K.E. *Peat Stratigraphy and Climatic Change*; Balkema Press: Rotterdam, The Netherlands, 1981.
50. Overbeck, F. Studien zur Hochmoorentwicklung in Niedersachsen und die Bestimmung der Humifizierung bei stratigraphisch-pollenanalytischen Mooruntersuchungen. *Planta* **1947**, *35*, 1–56. [[CrossRef](#)]
51. Clymo, R.S. Peat growth. In *Quaternary Landscapes*; Shane, I.C.K., Cushing, E.J., Eds.; Belhaven Press: London, UK, 1991; pp. 76–112.
52. Payne, R.J.; Blackford, J.J. Peat humification and climate change: A multi-site comparison from mires in south-east Alaska. *Mires Peat* **2008**, *3*, 1–11.
53. Yeloff, D.; Maquoy, D. The influence of vegetation composition on peat humification: Implications for palaeoclimatic studies. *Boreas* **2006**, *35*, 662–673. [[CrossRef](#)]
54. Shumilova, L.V. *Botanical Geography of Siberia*; Tomsk University Press: Tomsk, Russia, 1966; 430p.
55. Bond, G.; Kromer, B.; Beer, J.; Muscheler, R.; Evans, M.N.; Showers, W.; Hoffmann, S.; Lotti-Bond, R.; Hajdas, I.; Bonani, G. Persistent Solar Influence on North Atlantic climate during the Holocene. *Science* **2001**, *294*, 2130–2136. [[CrossRef](#)]
56. Steinhilber, F.; Beer, J.; Fröhlich, C. Total solar irradiance during the Holocene. *Geophys. Res. Lett.* **2009**, *36*, L19704. [[CrossRef](#)]
57. Zigert, H.G. Mineral formation in the area of permafrost. In *Structure and Thermal Regime of Sear Rocks*; Katasonova, E.G., Pavlov, A.V., Eds.; Nauka Press: Novosibirsk, Russia, 1981; pp. 14–21.
58. Rogov, V.V. *Fundamentals of Cryogenesis (Educational Manual)*; Academic publishing house “GEO”: Novosibirsk, Russia, 2009.
59. Velichko, A.A.; Timireva, S.N.; Kremenetski, K.V.; MacDonald, G.M.; Smith, L.C. West Siberian Plain as a late glacial desert. *Quat. Int.* **2011**, *237*, 45–53. [[CrossRef](#)]
60. Vink, A.; Steffen, L.; Reinhard, L.; Kaufmann, G. Holocene relative sea-level change, isostatic subsidence and the radial viscosity structure of the mantle of northwest Europe (Belgium, the Netherlands, Germany southern North Sea). *Quat. Sci. Rev.* **2007**, *26*, 3249–3275. [[CrossRef](#)]
61. Engelhart, S.E.; Horton, B.P.; Kopp, R.E.; Nelson, A.R.; Vacchi, M. A sea-level database for the Pacific coast of central North America. *Quat. Sci. Rev.* **2015**, *113*, 78–92. [[CrossRef](#)]
62. Baranskaya, A.V.; Khan, N.S.; Romanenko, F.Q.A.; Roy, K.; Peltier, W.R.; Horton, B.P. A postglacial relative sea-level database for the Russian Arctic coast. *Quat. Sci. Rev.* **2018**, *199*, 188–205. [[CrossRef](#)]
63. Baranskaya, A.V.; Zakharov, A.L.; Sorokovikov, V. Holocene sea-level changes in the Russian arctic, and sediments of laides and shallow bays as their indicators. In *Routes of Evolutionary Geography. Proceedings of the 2nd Scientific Conference in Memory of Prof. A.A. Velichko (Moscow, November 22-25, 2021)*; Institute of Geography RAS Press: Moscow, Russia, 2021; pp. 32–36.
64. Stein, R.; Niessen, F.; Dittmers, K.; Levitan, M.; Schoster, F.; Simstich, J.; Steinke, T.; Stepanets, O.V. Siberian river run-off and Late Quaternary glaciation in the southern Kara Sea, Arctic ocean: Preliminary results. *Polar Res.* **2002**, *21*, 315–322. [[CrossRef](#)]
65. Janssens, J.A.; Hansen, B.C.S.; Glaser, P.H.; Whitlock, C. Development of Raised-Bog Complex. In *The Patterned Peatlands of Minnesota*; Wright, H.E., Jr., Coffin, B., Aeseng, N.E., Eds.; University of Minnesota Press: Minneapolis, MN, USA; London, UK, 1992; pp. 189–221.
66. Pastukhov, A.; Marchenko-Vagapove, T.; Loiko, S.; Kaverin, D. Vulnerability of the Ancient Peat Plateaus in Western Siberia. *Plants* **2021**, *10*, 2813. [[CrossRef](#)]

- 
67. Kaufman, D.; KcKay, N.; Routson, C.; Erb, M.; Dätviler, C.; Sommer, P.S.; Heiri, O.; Davis, B. Holocene global mean surface temperature, a multi-method reconstruction approach. *Sci. Data* **2020**, *7*, 201. [[CrossRef](#)]
  68. Wanner, H.; Solomina, O.; Grosjean, M.; Ritz, S.P.; Jetel, M. Structure and origin of Holocene cold events. *Quat. Sci. Rev.* **2011**, *30*, 3109–3123. [[CrossRef](#)]

**Disclaimer/Publisher’s Note:** The statements, opinions and data contained in all publications are solely those of the individual author(s) and contributor(s) and not of MDPI and/or the editor(s). MDPI and/or the editor(s) disclaim responsibility for any injury to people or property resulting from any ideas, methods, instructions or products referred to in the content.